# Clearance of protein aggregates during cell division

Shoukang Du[1,3], Yuhan Wang[1], Bowen Chen[1], Shuangshuang Xie[1], Kuan Yoow Chan[1,3], David C. Hay[4], Ting Gang Chew[1,2,3,5,#]

**Affiliations**

[1]The Zhejiang University-University of Edinburgh Institute, Zhejiang University School of Medicine, Zhejiang University, Haining 314400, China

[2]Department of Cardiology of the Second Affiliated Hospital, Zhejiang University School of Medicine, Zhejiang University, Hangzhou 310058, China

[3]College of Medicine and Veterinary Medicine, The University of Edinburgh, Edinburgh, EH4 2XR, UK

[4]Centre for Regenerative Medicine, Institute for Regeneration and Repair, University of Edinburgh, 5 Little France Drive, Edinburgh EH16 4UU, UK

[5]State Key Laboratory of Biobased Transportation Fuel Technology, Zhejiang University, Hangzhou 310027, China

#Correspondending author: Ting Gang Chew (tinggchew@intl.zju.edu.cn)

## Abstract

Protein aggregates are spatially organized and regulated in cells to prevent deleterious effects of proteostatic stress. Misfolding of proteins in the endoplasmic reticulum (ER) result in aggregate formation, but how the aggregates are processed especially during cell division is not well understood. Here, we induced proteostatic stress and protein aggregation using a proteostasis reporter, which is prone to misfolding and aggregation in the ER. Unexpectedly, we detected solid-like protein aggregates deposited mainly in the nucleus and surrounded by the ER membrane. The membrane-bound aggregates were then cleared as cells progressed through mitosis and cytokinesis. Aggregate clearance depended on Hsp70 family chaperones in the ER, particularly BiP, and proteasomal activity. The clearance culminated at mitotic exit and required cyclin-dependent kinase 1 (Cdk1) inactivation and ER reorganization but was independent of the anaphase-promoting complex (APC/C). Thus, dividing cells have the capacity to clear protein aggregates to maintain proteostasis in the newly divided cells, which could have implications for human disease development and aging.

## Introduction

Nascent polypeptides fold into three-dimensional structures to perform their biological functions (Hipp et al., 2019). Misfolded proteins tend to have their hydrophobic residues exposed and result in aggregation of proteins (Hartl et al., 2011). Intramolecular beta-sheets in some proteins are also structural elements prone for protein aggregation (Tyedmers et al., 2010). Protein misfolding and aggregation not only disrupt the native function of the protein but also could interfere other proteins' functions by co-aggregation (Olzscha et al., 2011; Woerner et al., 2016). This challenges proteome

homeostasis (proteostasis) and causes proteostatic stress in cells, which is a main driver of cellular aging and neurodegenerative disorders (Balch et al., 2008; Labbadia and Morimoto, 2015).

Cells evolve several protein quality control (PQC) systems to maintain their proteostasis in which components of PQC systems facilitate refolding, degradation, and spatial deposition of misfolded protein aggregates (Jayaraj et al., 2020). Molecular chaperones are key players in the PQC system. They are involved to fold nascent polypeptides, target misfolded proteins for degradation by ubiquitin-proteasome system or autophagy, and promote solubilization of protein aggregates (Tyedmers et al., 2010). Eukaryotic cells confine misfolded proteins and smaller aggregates into distinct cellular deposition sites, which reduce the reactivity of these harmful species to the proteome (Kaganovich et al., 2008). These deposition sites include aggresomes or aggresome-like induced structures locating near centrosomes, INQ (intranuclear quality control compartment) residing in the nucleus, cytosolic CytoQ, and the perivacuolar IPOD (insoluble protein deposit) (Kaganovich et al., 2008). Confinement of protein aggregates in a deposition site facilitates retention of aggregates in short-lived cells (mother cells) during asymmetric cell division (Aguilaniu et al., 2003; Fuentealba et al., 2008; Rujano et al., 2006; Singhvi and Garriga, 2009; Zhou et al., 2014).

The endoplasmic reticulum (ER) processes one-third of cellular proteome and possesses stronger ability to maintain aggregation-prone proteins in a non-toxic state than the cytosol owing to its specific molecular chaperone environment (Vincenz-Donnelly et al., 2018). Chaperones in the ER such as HSPA5/BiP regulates the unfolded protein response (UPR), which blocks instant protein synthesis and activates transcription of genes involved in PQC (Preissler and Ron, 2019; Wiseman

et al., 2022). In addition, the proteostatic stress in the ER triggers ER-associated degradation (ERAD) and ER-phagy to remove misfolded proteins (Mochida and Nakatogawa, 2022; Olzmann et al., 2013). Despite the high capacity of proteostatic stress response in the ER (Rousseau et al., 2004; Vincenz-Donnelly et al., 2018), excessive misfolded proteins still lead to formation of protein aggregates in the ER (Melo et al., 2022; Miyata et al., 2020). In response to protein aggregation in the ER, BiP functions as a disaggregase to promote solubilization of these aggregates. In cells undergoing asymmetric cell division such as in the budding yeast, the ER diffusion barrier and the ER stress surveillance (ERSU) pathway ensure ER protein aggregates are retained preferentially in the short-lived mother cells during cell division (Clay et al., 2014; Pina and Niwa, 2015). How ER protein aggregates are regulated in dividing cells, especially those that do not undergo asymmetric cell division, is less well studied. We addressed the fate of ER protein aggregates in human cells undergoing cell division symmetrically and identified a clearance mechanism of protein aggregates when cells are exiting mitosis.

## Results

### Targeting a proteostasis reporter to the ER results in protein aggregate formation in the nucleus.

To investigate how cells maintain their proteostasis during cell division, we employed a proteostasis reporter consists of a firefly luciferase mutant prone for protein mis-folding and protein aggregation fused to a green fluorescent protein (FlucDM-eGFP) (Gupta et al., 2011). Next, we targeted the reporter to the ER by fusing a ER-targeting sequence at its N-terminus (ER-FlucDM-eGFP). Interestingly, we found that ER-FlucDM-eGFP assembled into visible protein aggregates in the

89 nucleus when stably expressed in mammary epithelial MCF10A cells in the absence of any
90 perturbation of the proteome stability (Figure 1A). The protein aggregates were below detection limit
91 of our microscopy in first 2 days after lentivirus transduction but progressively accumulated in cells
92 and stabilized in the population several days after lentivirus transduction. This contrasted with a
93 previous study in which the ER-FlucDM-eGFP was transiently expressed in cells and hence did not
94 allow long term tracking of the protein (Sharma et al., 2018). ER-FlucDM-mCherry localized to the
95 ER network indicated by the ER membrane protein Sec61β (Figure 1B). Since we detected
96 aggregate formation in the nucleus in cells expressing ER-FlucDM-eGFP, we tested if targeting
97 FlucDM-eGFP to the nucleus (NLS-FlucDM-eGFP) would result in the formation of visible protein
98 aggregates. Our data showed that NLS-FlucDM-eGFP did not form protein aggregates in the nucleus
99 and was not co-localized with the ER-FlucDM-mCherry, and accumulated lower protein abundance
100 than ER-FlucDM-eGFP (Figure S1A-D). Luciferase activity measurement showed that ER-FlucDM-
101 eGFP has significantly reduced enzymatic activity and was not functional possibly due to mis-folding
102 and protein aggregation (Figure 1C). ER-FlucDM-eGFP was also detected in the insoluble fraction
103 after heat stress (Figure S1E). Moreover, we observed the colocalization of ER-FlucDM-eGFP
104 aggregates and thioflavin T (ThT), a universal dye to detect amyloid fibril, further supporting these
105 aggregates were misfolded protein aggregates (Figure S1F). Thus, expression of ER-FlucDM-eGFP
106 results in proteostatic stress and allows us to study how protein aggregates are regulated in human
107 cells.
108
109 Formation of protein aggregates in the nucleus by ER-FlucDM-eGFP was not limited to MCF10A
110 cells. The protein aggregates were also detected in the nucleus when ER-FlucDM-eGFP was

111 expressed in other cell lines such as A549, MDA-MB-231 and U2OS cells (Figure 1A and S1G).
112 Similar observations were found when a different N-terminal signal peptide sequence was used
113 (Figure 1D and S1H). In addition, when ER-FlucDM was replaced by ER-HaloDM, which is a
114 modified haloalkane dehalogenase prone to mis-folding and aggregation (Melo et al., 2022), we
115 observed similar protein aggregates in the nucleus (Figures 1D and S1H). However, only very low
116 number of cells formed aggregates in the nucleus when intact GFP was targeted to the ER (Figure
117 S1I). Thus, ER-FlucDM-eGFP formed protein aggregates in the nucleus independent of cell line,
118 fluorescent protein types, specific ER targeting sequence and FlucDM.
119
120 Despite localizing in the nucleus, we found that the protein aggregates were surrounded by the ER
121 membrane as stained by the ER-tracker (Figure 1E). To further confirm this, we sectioned the cells
122 and used electron microscopy to observe the protein aggregates. We found that the aggregates
123 were surrounded by a single layer membrane closed to the inner membrane of the nucleus (Figure
124 1F). Thus, the aggregates are intra-nuclear membranous structure surrounded by the ER membrane.
125
126 **Differential and slow turnover of protein aggregates in cells at interphase and mitosis.**
127 Pathological proteins aggregates such as Z-α1-antitrypsin accumulated in the ER exhibited minimal
128 turnover (Dickens et al., 2016). To test whether ER-FlucDM-eGFP aggregates has a reduced
129 dynamics as well, we performed fluorescence recovery after photobleaching (FRAP) in cells
130 expressing both ER-FlucDM-eGFP and ER-FlucDM-mCherry. The ER-FlucDM-eGFP signal served
131 as a tracker for the location of aggregates and the ER-FlucDM-mCherry was used to probe the
132 aggregate dynamics. We photobleached ER-FlucDM-mCherry with 561 nm laser while ensuring ER-

133 FlucDM-eGFP signal was not affected. In interphase cells, ER-FlucDM-mCherry aggregates
134 intensity barely recovered after 4.5 min post-bleaching, indicating that ER-FlucDM-mCherry
135 aggregates possessed minimal turnover similar to that of in other protein aggregates such as Z-α1-
136 antitrypsin (Figure 2A). Similarly, ER-HaloDM-eGFP aggregates in the nucleus also displayed low
137 recovery after photobleaching (Figure S2A). When ER-FlucDM-mCherry aggregates were
138 photobleached in mitotic cells, the recovery of intensity was also much lesser than the ER-FlucDM-
139 mCherry signal present in the ER network (Figures 2B and 2C). However, ER-FlucDM-mCherry
140 aggregates in mitotic cells showed a higher recovery than that of in interphase cells (Figure 2D;
141 aggregates of interphase cells recovered from 0.131 ± 0.093 to 0.157 ± 0.095; aggregates of mitotic
142 cells recovered from 0.196 ± 0.137 to 0.356 ± 0.151).
143
144 Consistently, the single-cell analysis revealed that in mitotic cells, there was an increase of the
145 recovery intensity of ER-FlucDM-mCherry in late time-point as compared to that of in early time-
146 points after photobleaching. The increased recovery intensity was not observed in ER-FlucDM-
147 mCherry aggregates of interphase cells (Figure S2B). Taken together, ER-FlucDM-mCherry
148 aggregates in the nucleus have low turnover and the aggregate displays increased turnover in mitotic
149 cells.
150
151 **Protein aggregates are cleared during cell division.**
152 Since aggregates displayed some levels of turnover during mitosis (Figures 2B, 2C and 2D), we next
153 investigated the aggregate behaviour throughout cell division. To this end, we labelled cells
154 expressing ER-FlucDM-eGFP with SiR-Tubulin to distinguish cells at various stages based on the

155 microtubule organization. We categorized cells into interphase and prophase, prometaphase,
156 metaphase, anaphase, telophase and early G1 cells based on their microtubule structures (Figure
157 3A). Next, we analyzed the number and area of aggregates in cells of each category. Interestingly,
158 we observed that the number and area of aggregates in telophase and early G1 cells were
159 significantly lower than in interphase cells, suggesting that aggregates are cleared gradually when
160 cells progress through mitosis and cytokinesis (Figure 3B).
161
162 To test whether this was the case, we employed time-lapse imaging to profile aggregates in cells
163 undergoing division. To increase the number of dividing cells during imaging, we synchronized cells
164 at G2/M and released them into mitosis prior to imaging. We observed that upon entry into mitosis,
165 the ER-FlucDM-eGFP aggregates were released from the nucleus during nuclear envelope
166 breakdown and gradually decreased in numbers as cells progress through mitosis and cytokinesis
167 (Figure 3C and Video 1). In majority of early divided G1 cells, there was essentially no detectable
168 aggregates (Figure 3D). Interestingly, the aggregates released from the nucleus during mitosis were
169 still surrounded by the ER membrane as indicated by the ER-tracker (Figures S3A and S3B). The
170 decrease of aggregates appears to happen specifically in dividing cells as the number and area of
171 aggregates remained largely unchanged in interphase cells (Figures 3C and 3D). Furthermore,
172 aggregates formed in cells expressing ER-HaloDM-eGFP decreased in numbers when cells
173 progress through mitosis and cytokinesis (Figure S3C and Video 2), suggesting that the clearance
174 of protein aggregates during cell division was not specific to ER-FlucDM-eGFP.
175
176 **Effects of ER stress inducers on aggregate clearance in mitotic cells**.

177 Expression of ER-FlucDM-eGFP results in proteostatic stress in cells. Consistently, we observed
178 that gene expression for chaperones and co-chaperones in the ER were upregulated in these cells
179 (Figure 4A), indicating cells involved ER proteostasis control during adaptation. Proteomic analysis
180 of cells expressing ER-FlucDM-GFP showed up-regulation of proteins involved in ER stress
181 response (Figure S4A). We speculated that acute perturbation to ER homeostasis could exacerbate
182 the proteostatic stress in dividing cells expressing ER-FlucDM-eGFP and affect aggregate clearance
183 during mitosis. To test if this was the case, synchronized cells expressing ER-FlucDM-eGFP were
184 released into mitosis in the presence of either DMSO (control) or 1 μM thapsigargin (Thaps), which
185 blocks the ER calcium ion pump and causes ER stress. In cells at prometaphase and metaphase
186 (35 min after release), DMSO and Thaps treatments showed comparable number and area of
187 aggregates in cells (Figures 4B and 4C). However, in cells at the late stage of cell division (65 min
188 after release), there were significantly higher number of aggregates retained in the cytosol of Thaps-
189 treated cells than DMSO (Figures 4B and 4C). Consistently, time-lapse microscopy revealed that
190 ER-FlucDM-eGFP aggregates retained in the cytosol after cytokinesis in Thaps-treated cells,
191 whereas the aggregates were largely cleared in control cells completing cytokinesis (Figures 4D, 4E,
192 S4B and Video 4). Thus, acute treatment of ER stress inducer Thaps in dividing cells prevents
193 clearance of ER-FlucDM-eGFP aggregates.
194
195 A previous study showed that cells with protein aggregates treated for hours with Thaps or
196 Tunicamycin (Tuni), which inhibits protein glycosylation in the ER, promotes aggregate clearance in
197 cells (Melo et al., 2022). To test if prolonged treatment of cells expressing ER-FlucDM-eGFP with
198 Tuni could promote aggregate clearance, we pretreated cells blocked at G2/M with varying

concentrations of Tuni for 3 hours and released cells into mitosis. Interestingly, prolonged pretreatment of Tuni prior to mitosis promoted aggregate clearance in dividing cells (Figure S4C). Thus, acute treatment of cells expressing ER-FlucDM-eGFP with ER stress inducers prevents aggregate clearance in dividing cells while prolonged treatment with ER stress inducers promotes aggregate clearance.

**Hsp70 family protein BiP is required for aggregate clearance during cell division.**

Since we observed that the expression of a chaperone Hsp70 (HSPA5/BiP) was upregulated in cells expressing ER-FlucDM-eGFP (Figure 4A) and Hsp70 is involved in elimination of protein aggregates (Melo et al., 2022; Nillegoda et al., 2015), we next tested whether the clearance of ER-FlucDM-eGFP aggregates in dividing cells was mediated by Hsp70 family proteins. To this end, cells entering mitosis were treated with either DMSO (control) or VER-155008 (VER), an inhibitor of HSP70's ATPase activity (Samanta et al., 2021). We found that VER-treated dividing cells fixed after 65 minutes released from the G2/M boundary retained high number of ER-FlucDM-eGFP aggregates in the cytosol compared to control treatment (Figures 5A and 5B). Time-lapse microscopy showed that when cells were treated with VER, ER-FlucDM-eGFP aggregates released from the nucleus upon entry into mitosis were not cleared as to the same extent as control cells (Figure 5C and Video 5).

HSPA5/BiP is a major Hsp70 family member in regulating ER proteostasis. We next tested whether inhibition of BiP function could affect clearance of aggregates in dividing cells. Similar to VER treatment, inhibition of BiP's ATPase activity by YUM-70 (Samanta et al., 2021) led to a dose-

221 dependent accumulation of ER-FlucDM-eGFP aggregates in cells (Figures 5D and 5E). Moreover,
222 by using immunofluorescence staining, we found a strong colocalization of BiP and ER-FlucDM-
223 eGFP, consistent with a role of BiP in regulating ER-FlucDM-eGFP aggregates (Figures S5A to S5C).
224 Collectively, our data demonstrated that the clearance of ER-FlucDM-eGFP aggregates was
225 regulated by the HSP70 family proteins, particularly BiP.
226
227 **Aggregate clearance is a mitotic exit event but is independent of the anaphase promoting**
228 **complex (APC/C)**.
229 Protein aggregates are subjected to proteasomal degradation in cells (Tyedmers et al., 2010). To
230 test if aggregate clearance during cell division involves proteasomes, we inhibited the proteasome
231 activity with MG132 in dividing cells expressing ER-FlucDM-eGFP. After treating cells released from
232 the G2/M boundary with low or high concentrations of MG132 for 55 minutes, majority of mitotic cells
233 were arrested at metaphase and accumulated high number of aggregates as compared to control
234 cells treated with DMSO (Figures S6A and S6B). Next, we inhibited the proteasome with MG132 in
235 cells at late anaphase or telophase and examined the aggregates 35 minutes after MG132 treatment
236 (Figures S6C and S6F). In cells completing cytokinesis, there were significantly high number of
237 aggregates in the early divided cells treated with MG132 versus the control (Figures S6D, 6E, S6G
238 and S6H).
239
240 Since protein aggregates are cleared when cells progress through mitosis and cytokinesis, which
241 are the cell cycle stage with low Cyclin B/CDK1 activity, we speculated that inactivation of CDK1
242 activity in MG132-treated and metaphase-arrested cells could lead to clearance of ER-FlucDM-

243 eGFP aggregates in the cytosol. To test if this was the case, we released cells into mitosis in the
244 presence of MG132 for 55 minutes and treated metaphase-arrested cells with RO-3306 to inhibit
245 Cdk1 activity (Figure 6A). Interestingly, ER-FlucDM-eGFP aggregates were cleared in cells treated
246 with RO-3306 while the aggregates were retained in cells treated with DMSO (Figures 6B and S6I).
247 Consistently, live cell imaging demonstrated similar accelerated clearance in Cdk1 inhibited cells
248 (Figures 6C and 6D). Thus, clearance of the aggregates happens when cells exit from mitosis.
249
250 We established that clearance of aggregates during cell division requires proteasomes and CDK
251 inactivation, it is possible that the anaphase promoting complex (APC/C), which is a E3 ubiquitin
252 ligase regulating mitotic exit (Watson et al., 2019), is involved in clearing the aggregates. To test if
253 this was the case, we inhibited APC/C activity using a cocktail of APC/C inhibitors (APC/Ci) consists
254 of Apcin and ProTAME in dividing cells expressing ER-FlucDM-eGFP (Sackton et al., 2014).
255 Interestingly, inhibition of APC/C did not affect aggregate clearance as APC/Ci-treated cells that have
256 arrested at metaphase have comparable number of aggregates as in control DMSO-treated cells
257 (Figures 6E and 6F). When cells at late anaphase or telophase were treated with APC/Ci, the newly
258 divided cells have similar number of aggregates as in control cells (Figures 6G, 6H and 6I). Lastly,
259 we verified the efficacy of APC/C inhibition using cells expressing the APC/C reporter derived from
260 Geminin (Figure S6J). Consistently, APC/Ci treatment has prevented the removal of APC/C reporter
261 in newly divided cells indicating that the APC/C was inhibited by the dosage of APC/Ci used in our
262 experiments (Figure S6K). Taken together, our data showed that clearance of ER-FlucDM-eGFP
263 aggregates happens when cells exit from mitosis, is proteasome dependent but does not involve
264 APC/C.

To examine if ER-FlucDM-eGFP decreased in abundance while cells progressing through mitosis, we inhibited protein translation using cycloheximide (CHX) in cells released from G2/M boundary. Short half-life proteins like p53 showed a rapid decrease of abundance upon CHX treatment, indicating CHX prevented new protein synthesis in our treatment (Figure S7A and S7B). ER-FlucDM-eGFP did not show significant change of its abundance after CHX treatment, suggesting that ER-FlucDM-eGFP aggregates were not cleared by the protein degradation mechanism directly (Figure S7A and S7C). Consistently, when the total GFP intensity of ER-FlucDM-eGFP was quantitated in dividing cells 20-30 min (early) or 85-95 min (late) released from G2/M boundary, there was no significant change of GFP fluorescence intensity between early and late dividing cells (Figure S7D), further supported that the protein degradation mechanism was not responsible for the ER-FlucDM-eGFP aggregate clearance.

**Aggregate clearance depends on the ER reorganization during cell division**

Since we showed that ER-FlucDM-eGFP aggregates are not primarily cleared by the protein degradation mechanism, we considered the possibility that aggregate clearance requires reorganization of the ER that happens in cells exiting mitosis. To this end, we used CRISPR interference (CRISPRi) technique to knock down ER membrane fusion proteins Atlastin 2 (ATL2) and Atlastin 3 (ATL3) in cells expressing ER-FlucDM-eGFP and quantitated the aggregate numbers in cells exiting mitosis (65 min after release). Interestingly, dividing cells depleted of ATL2 and ATL3 accumulated more ER-FlucDM-eGFP aggregates than in control cells (Figure 7A and B).

287 The mitotic kinase Aurora A has been recently shown to remodel the ER network during mitosis
288 (Zhang et al., 2024). We next tested if blocking Aurora A activity could affect aggregate clearance.
289 When mitotic cells expressing ER-FlucDM-eGFP were treated with Aurora A inhibitor, MLN-8237,
290 aggregate clearance was prevented compared to cells treated with DMSO (Figure 7C and D). Since
291 the ER reorganization involves microtubule dynamics, we also perturbed microtubule networks by
292 treating cells expressing ER-FlucDM-eGFP by nocodazole (Figure 7E and F). Our data showed that
293 mitotic cells treated with nocodazole accumulated higher number of aggregates. Taken together, we
294 found that clearance of ER-FlucDM-eGFP aggregates involves reorganization of the ER during
295 mitotic exit (Lee et al., 1989).
296

297 **Discussion**

298 We showed that stably expression of ER-FlucDM-eGFP leads to proteostatic stress and formation
299 of protein aggregates in human cells without the use of additional proteostatic stressors. ER-FlucDM-
300 eGFP aggregates may derive from the invagination of the inner nuclear membrane. Morris et al
301 reported a similar aggregate upon BiP overexpression (Morris et al., 1997). This fluorescent based
302 live-cell imaging reporter enables us to study how protein aggregates are regulated in dividing cells,
303 which are sensitive to genetic or environmental perturbations. Conventional methods that use
304 proteasomal inhibitors to cause proteome imbalance are not ideal to investigate proteostasis in
305 dividing cells given an essential role of protesomes in driving mitotic exit (Ghislain et al., 1993;
306 Glotzer et al., 1991). Additionally, methods such as heat shock also perturb mitotic progression,
307 especially in human cells (Kakihana et al., 2019). By using ER-FlucDM-eGFP that does not perturb
308 cell cycle progression significantly, we reveal an unexpected process of clearing protein aggregates

309 in cells progressing through mitosis and cytokinesis.

310

311 Previous studies showed that the proteome of mitotic cells have higher structural stability and less
312 aggregation prone compared to that of in interphase cells (Becher et al., 2018; Wirth et al., 2013).
313 Post-translational modifications such as phosphorylation of mitotic proteins are suggested to be
314 responsible for the protein stability during cell division (Becher et al., 2018). The aggregate clearance
315 we identified in this study could represent an active mechanism that increases proteome stability in
316 dividing cells. We found that aggregate clearance requires Cdk1 inactivation, which is a hallmark of
317 mitotic exit, however, does not involve APC/C that is important in driving mitotic exit through protein
318 degradation. It is possible that APC/C targets mostly cytosolic proteins whereas ER-FlucDM-eGFP
319 aggregates are confined in a membrane during mitosis. Furthermore, the clearance of protein
320 aggregates coincides with ER reorganization that happens throughout mitosis and cytokinesis, which
321 may contribute to the aggregate clearance (Bergman et al., 2015; Schlaitz et al., 2013). A previous
322 study showed that the size of protein aggregates is limited by the ER tubules (Parashar et al., 2021).
323 In fact, when the ER reorganization is perturbed by depleting ER membrane fusion proteins ATL2
324 and 3, clearance of ER-FlucDM-eGFP aggregates is affected. Consistently, ER-FlucDM-eGFP
325 proteins do not turn over significantly in cells progressing through mitosis and cytokinesis. Thus, it is
326 less likely that ER-FlucDM-eGFP is ubiquitinated by APC/C and targeted for protein degradation.

327

328 Misfolded or damaged proteins form protein aggregates and are spatially organized into specific
329 subcellular sites to sequester them from other cellular processes (Hill et al., 2017). These aggregate
330 deposition sites are localized in the cytosol or in the nucleus to confine misfolded proteins and

aggregates for elimination from cells (Kaganovich et al., 2008). Similarly, we identified confinement of ER-FlucDM-eGFP aggregates in the nucleus and are surrounded by a single layer membrane. These intranuclear membranous structures contain ER membranes and BiP, which is a key Hsp70 family chaperone in the ER and translocates into the nucleus under stress (Liu et al., 2023). How protein aggregates are targeted and assembled into the intranuclear membranous structure awaits future investigation. Interestingly, upon entry into mitosis, concomitant with the nuclear membrane breakdown, the membranous structure is released from the nucleus and the aggregates are cleared when cells progress though mitosis till early G1 phase of the daughter cells. The confinement and clearance of protein aggregates during cell division presumably protect dividing cells from harmful effects of protein misfolding and aggregation and to ensure reliable inheritance of genetic materials. It has been reported that aggregates are asymmetrically retained in one of the daughter cells that are usually short-lived (Rujano et al., 2006). The aggregate clearance mechanism we report here may provide an additional cellular defense strategy to overcome proteostatic stress and to maintain proteome integrity during cell division. Proteomic analysis of cells expressing ER-FlucDM-eGFP identified up-regulation of multiple proteins involved in ER stress response, indicating that cells experience significant proteostatic stress upon expression of ER-FlucDM-eGFP. Moreover, several proteins regulating cell cycle displayed higher abundance in the proteome, which together with proteostatic stress indicate a perturbed cellular health.

Hsp70 chaperones regulate proteostasis by preventing protein aggregation, promoting disaggregation and subjecting solubilized aggregates to degradation or refolding (Rosenzweig et al., 2019). Our proteomic analysis revealed significant expression of BiP (HSPA5) in cells expressing

353 ER-FlucDM-eGFP but not other Hsp70 family members. A recent study showed that BiP solubilizes
354 aggregates and drives aggregate clearance in the ER (Melo et al., 2022). Our study of mitotic
355 aggregate clearance in dividing cells further extend the role of BiP in disaggregation. Consistently,
356 we found that Cdk1 inactivation in the presence of the proteasomal inhibitor could still lead to
357 aggregate clearance, suggesting a partial role of the proteosome in clearing aggregates and the
358 disaggregation breaks down the aggregates into smaller and possibly soluble species. The role of
359 proteasome in regulating ER-FlucDM-eGFP aggregate clearance appears indirect as ER-FlucDM-
360 eGFP proteins are stable throughout cell division. It is possible that players involved in ER-FlucDM-
361 eGFP aggregate clearance are regulated by proteasomal degradation, which are affected when
362 proteasomes are inhibited. Interestingly, Melo et al. showed that aggregate clearance is promoted
363 by treating ER-cells with ER stressors as the treatment triggers UPR, which in turn leads to higher
364 activity of BiP to cope with the ER stress. We observed differential responses of aggregate clearance
365 to ER stressors depending on the duration of the treatments. It is possible that acute treatment of
366 the ER stressor on dividing cells does not provide sufficient time for cells to accumulate abundant
367 amount of BiP given that mitotic cells are not very transcriptionally active (Palozola et al., 2017). Also,
368 degradation of BiP could be accelerated upon the treatment of ER stressors, which in turn
369 undermines the abundance of BiP in disaggregation (Shim et al., 2018). Thus, short term treatment
370 of the ER stressor in cells exacerbates the ER stress and affects aggregate clearance during cell
371 division, whereas longer treatment of the ER stressor promotes aggregate clearance. Mechanistic
372 understanding of aggregate clearance during cell division could offer new insights to understand
373 disaggregation in proteostasis control.
374

375 **Materials and methods**

376 **Cell lines and culture**

377 MCF10A cells were cultured in DMEM F-12 (Sigma) supplemented with 1% Glutamax (Gibco), 5%
378 horse serum (Biological Industries), 20 ng/ml EGF (Gibco), 0.5 mg/ml Hydrocortisone
379 (MedChemExpress), 100 ng/ml Cholera toxin (Sigma), 10 μg/ml Insulin (Biological Industries), and
380 1% Pen/Strep (Biological Industries). U2OS, A549, and HEK293Ta cells were maintained in DMEM
381 (Sigma) with Glutamax (Gibco), 6% fetal bovine serum (Biological Industries), and 1% Pen/Strep
382 (Biological Industries). MDA-MB-231 cells were cultured in DMEM F-12 (Sigma) with 1% Glutamax
383 (Gibco) and 1% Pen/Strep (Biological Industries). All cell cultures were maintained at 37°C with 5%
384 $CO_2$ in a humidified incubator. Cells expressing ER-FlucDM-eGFP, ER-eGFP, ER-HaloDM-eGFP,
385 ER-FlucWT-eGFP, and $ER^{FSHR}$-FlucDM-eGFP, ER-FlucDM-mCherry, NLS-FlucDM-eGFP were
386 generated through lentivirus transduction and selected with 5 μg/mL puromycin (Sangon Biotech).
387 MCF10A cells expressing mStayGold-Sec61β were prepared by lentivirus transduction, selected
388 with 50 μg/mL hygromycin B and only used in three days after transduction (Ando et al., 2024).
389 MCF10A cells expressing CRISPRi plasmids to knock down ATL2 and ATL3 were selected by 6
390 μg/mL Blasticidin (Solarbio, 703X023) and only used in five days after transduction. MCF10A cells
391 co-expressing ER-FlucDM-eGFP and ER-FlucDM-mCherry for FRAP or co-expressing ER-FlucDM-
392 mCherry and mGreenLantern-hGeminin (degron) or co-expressing ER-FlucDM-mCherry and NLS-
393 FlucDM-eGFP were generated by lentivirus transduction and selected by 5 ug/mL puromycin and
394 followed by fluorescence-activated cell sorting (FACS) to enrich double-positive cells.

395

396 **Lentivirus packaging**

397 Lentiviral particles were generated using the 3rd generation lentiviral packaging system. Packaging
398 plasmids pRSV-Rev, pMDLg/pRRE, pMD2.G (kindly provided by Didier Trono) and the transfer
399 plasmid were chemically transfected using GeneTwin transfection reagent (Biomed, TG101) into the
400 HEK293Ta packaging cell line (Genecopoeia, LT008). The cell culture medium was harvested after
401 2 days and filtered through a 0.45 μm filter. The filtrate was concentrated using a 5X precipitation
402 solution (250 g/L PEG 8,000 and 43.83 g/L NaCl in $ddH_2O$) for overnight, and precipitated by
403 centrifuging at 4000 × g for 25 min at 4°C. Lentiviral particles were resuspended in phosphate
404 buffered saline (PBS) and added to the culture medium, which were supplemented with 1 μg/mL
405 polybrene (HanBio).
406
407 **Lentivirus expression constructs**
408 Lentiviral transfer plasmids used in this study were listed below: pTGL0563 containing FlucDM-eGFP
409 in which FlucDM was mutated from FlucWT (a gift from Dr. Mikael Bjorklund); pTGL0645 containing
410 ER-FlucDM-eGFP-KDEL; pTGL0662 containing NLS-FlucDM-eGFP; pTGL0673 containing ER-
411 FlucDM-mCherry-KDEL; pTGL0698 containing ER-FlucWT-eGFP-KDEL; pTGL0703 containing ER-
412 HaloDM-eGFP-KDEL in which HaloDM was mutated from HaloWT; pTGL0707 containing ER-
413 HaloWT-eGFP-KDEL; pTGL0733 containing ER-eGFP-KDEL; pTGL0743 containing $ER^{FSHR}$-
414 FlucDM-eGFP; pTGL0828 containing mGreenLantern-hGeminin (degron); pTGL0891 was the
415 empty plasmid used in constructing pTGL0645 and used as a control for proteomics; pTGL0914
416 containing mStayGold-Sec61β; pTGL0386 was the empty plasmid in constructing CRISPRi plasmids;
417 pCRISPRi0249 to knockdown ATL2 containing gRNA 5' GAGGGCAGCAACCGCACCAG 3';
418 pCRISPRi0252 to knockdown ATL3 containing gRNA 5' GAGCAGGGGTGCAGAGGAGA 3'.

419

420 **Quantitative real-time PCR (qPCR)**

421 Total RNA was extracted from cells using the FastPure Cell/Tissue Total RNA Isolation Kit V2
422 (Vazyme, RC112-01). Subsequently, the RNA was reversely transcribed into complementary DNA
423 (cDNA) using the HiScript II Q RT SuperMix for qPCR (Vazyme, R223-01). The levels of the cDNAs
424 were quantified using real-time PCR with the ChamQ Universal SYBR qPCR Master Mix (Vazyme,
425 Q711-02). The PCR reaction mix was prepared on a hard-shell PCR plate (Bio-Rad, HSP9655),
426 sealed with Microseal 'B' seals (Bio-Rad, MSB1001), and conducted in the CFX96 Touch Real-Time
427 PCR Detection System (Bio-RAD, C1000). Primers used in the qPCR: GAPDH, 5'
428 CAGGAGGCATTGCTGATGAT 3' and 5' GAAGGCTGGGGCTCATTT 3'; HSPA5, 5'
429 CACAGTGGTGCCTACCAAGA 3' and 5' TGTCTTTTGTCAGGGGTCTTT 3'; Calreticulin, 5'
430 ATAAAGGTTTGCAGACAAGC 3' and 5' CCACAGTCGATGTTCTGCTC 3'; HSP90B1, 5'
431 TCCAGCAGAAAAGAGGCTGA 3' and 5' CAAATTCGGGAAGGGCCTGA 3'; CANX, 5'
432 GCACCTATTCTGGAGGCGAG 3' and 5' ACAGCAACCACTTCCCTTCC 3'; P4HB, 5'
433 TTCAGGAATGGAGACACGGC 3' and 5' TCCACGTCCTTGAAGAAGCC 3'; DNAJB9, 5'
434 GTGGAGGAGCAGCAGTAGTC 3' and 5' CGCTCTGATGCCGATTTTGG 3'; ATL2, 5'
435 CTGGTTCCATTGCTGCTTGC 3' and 5' CTTCAGCTGTTGCCTGAAGC 3'; ATL3, 5'
436 TCACCCCAAGTCCATGCTTC 3' and 5' CTCCCCCACAAACCTCTTCC 3'.. The $C_T$ value for
437 GAPDH was used for normalization to obtain the relative expression level.

438

439 Protein immunoblotting

440 Adherent cells were lysed with 1x LDS sample buffer (Beyotime) and boiled at 95°C for 10 min. The

441 1x LDS sample buffer was prepared by diluting 4 X LDS sample buffer (Beyotime) in 100 mM Tris-
442 HCl (pH 7.4) with 2.5% v/v β-mercaptoethanol. Protein samples were separated by pre-cast SDS-
443 PAGE gels (GenScript) and blotted to a PVDF membrane (EMD Millipore). Blots were blocked with
444 Quick Block buffer (Beyotime) for at least 20 min at room temperature and were incubated at 4°C
445 overnight with the primary antibody. After rinsing blots with TBS containing 0.05% Tween-20 for four
446 times (5 min each time), blots were incubated at room temperature with the secondary antibody for
447 1h, followed by washing with TBS containing 0.05% Tween-20. Odyssey CLX was employed to
448 image the blots and LI-COR Image Studio software was used to quantify the band intensity. To
449 incubate different primary antibodies in the same blot, the blot was vigorously rinsed with the
450 stripping buffer (CWBIO, 01427/12724) and washed 3 times with TBS containing 0.05% Tween-20
451 and processed as described before.
452
453 To examine the solubility of ER-FlucDM-eGFP in Figure S1E, the lysis buffer containing 100 mM
454 Tris-HCl (pH 7.4), 1% protease inhibitor cocktail (Lablead, C0101) and different concentrations of
455 NP-40 (Sigma) was used. To prepare supernatant and pellet fractions of ER-FlucDM-eGFP, cells
456 were lysed with the lysis buffer containing 0.2%, 0.5% or 1.0% v/v NP-40. The lysate was then
457 centrifuged at 14,000 ×g for 10 min at 4°C and the supernatant was collected. The cell pellet was
458 further lysed with 1x LDS buffer on ice for 40 min and vortexed vigorously for 10 seconds every 10
459 min.
460
461 Primary antibodies used were: 1:3000 anti-GFP (Huabio, ET1601-13); 1:5000 anti-β-actin (Genscript,
462 A00702); 1:1000 anti-Cyclin B1 (Proteintech, 55004-1-AP); 1:1000 anti-p53 (Huabio, ET1601-13).

463 Secondary antibodies were goat anti-Rabbit IgG (H+L) Highly Cross-Adsorbed Secondary Antibody
464 conjugated to Alexa Fluor™ Plus 800 (Invitrogen, A32735) and goat anti-Mouse IgG (H+L) Highly
465 Cross-Adsorbed Secondary Antibody conjugated to Alexa Fluor™ Plus 680 (Invitrogen, A32729)
466
467 Proteomics
468 MCF10A cells transduced with pTGL0891 (empty vector) or pTGL0645 (ER-FlucDM-eGFP) for six
469 days were trypsinized, centrifuged and washed twice with ice-cold PBS. The pellets were quickly
470 frozen by liquid nitrogen and then sent to Tsingke (Wuhan, China) for further processing for
471 proteomics. In brief, cell pellets were lysed with buffer containing 8 M urea, 1 mM PMSF and 2 mM
472 EDTA. Samples were subjected to ultrasound sonication on ice for five minutes and followed by
473 centrifugation at 15,000 xg for 10 minutes. The supernatants were then collected, and their
474 concentrations were measured using BCA method (Beyotime). Solutions containing 100 μg was
475 topped up to 200 μl with 8M urea and DTT (final concentration 5 mM) was added before incubation
476 at 37°C for 45 min. Protein samples were alkylated using iodoacetamide (final concentration 11 mM)
477 in a dark room at room temperature for 15 min. The solutions were then subjected to trypsin digestion
478 and further analyzed using LC-MS/MS analysis. The MS/MS data were processed using DIA-NN
479 (v1.8.1). The protein quantification of DIA-NN software is done by MaxLFQ algorithm.
480
481 **Luciferase activity test**
482 Each well of 96-well plates (Biosharp, BS-MP-96W for luminescence, BS-MP-96B for fluorescence)
483 was seeded with 10,000 cells in 100 μL of medium. After incubation for 18 hours, 5 μM MG132 was
484 added to the MG132+FlucDM-eGFP group, while other untreated wells remained unchanged.

485 Following an additional 6 hours, cells were washed once with PBS.

486

487 For luminescence detection, cell lysis was achieved by adding 50 μL of Steady-Glo Luciferase Assay
488 System buffer (Promega, E2510) to the wells, followed by a 15-minute incubation at room
489 temperature. Luminescence in each well was then recorded three times over 5 minutes using the
490 Spark® Multimode Microplate Reader (Tecan, 1000 ms exposure). Luminescence intensity in each
491 well was calculated by normalizing these three measurements and subtracting the background signal
492 from empty wells.

493

494 To determine abundance of luciferase in each treatments, 1 x $10^5$ MCF10A cells were seeded in 12-
495 well for 24 h. The cells were lysed with 1x LDS sample buffer (Beyotime) and protein immunoblotting
496 using anti-β-actin and anti-GFP, respectively was performed. β-actin was first used to normalized the
497 GFP intensity, and the value was used to normalize the luminescence to calculate the luciferase
498 activity.

499

500 **Mitotic cell preparation**

501 To increase the quantity of dividing cells, cells were first seeded on imaging chambers (ibidi, 80826)
502 and were synchronized to the G2/M boundary by treating cells with 7.5 μm RO-3306 (Selleckchem,
503 S7747) for 16 to 20 hours. Cells were released to enter into mitosis synchronously by washing once
504 with pre-warmed fresh medium.

505

506 **Drug treatments**

507 The following drugs were used in this study: Thapsigargin (Abcam, ab120286), Tunicamycin (GlpBio,
508 GC16738), MG132 (CSN Pharm, CSN11436), YUM70 (Aladdin, Y413413), VER-155008 (CSN
509 Pharm, CSN13116), Apcin (Sigma, SML1503), proTAME (Cayman Chemical, 25835),
510 Cycloheximide (AbMole, M4879), Nocodazole (Beyotime, S1765), MLN-8237 (TargetMol, T2241).
511

512 **Immunofluorescence staining**

513 For HSPA5/BiP staining, MCF10A cells expressing ER-FlucDM-eGFP were seeded in 8-well ibidi
514 plates, fixed with 100% methanol for 10 minutes and permeabilized with 0.5% Triton X-100 for 15
515 minutes. The fixed cells were blocked with 5% FBS in PBS for 30 minutes. Subsequently, cells were
516 incubated with the mouse anti-BiP antibody (HuaBio, HA601076) at 1:200 dilution in 1% FBS
517 overnight at 4°C. The secondary antibody used was Donkey Anti-Mouse IgG H&L (Alexa Fluor® 568,
518 ab175472, Abcam) at 1:2000 dilution for one hour. For Tubulin staining, cells were fixed using 4%
519 PFA for 20 minutes and permeabilized with 0.5% Triton X-100 for 15 minutes. After blocking the fixed
520 cells with 5% FBS in PBS for 30 minutes, cells were stained with the mouse anti-α-tubulin
521 monoclonal antibody (Proteintech, 66031-1-IG) at 1:200 dilution. The secondary antibody used was
522 Donkey Anti-Mouse IgG H&L (Alexa Fluor® 568, ab175472, Abcam) at 1:2000 dilution for one hour.
523 To stain DNA, DAPI Staining Solution (Sangon Biotech, E607303, 5 mg/L) was diluted in PBS to 50
524 ng/mL and applied to cells for 10 minutes. After the DAPI solution was removed, fixed cells were
525 washed with PBS twice before imaging.
526

527 **Transmission Electron Microscopy (TEM)**

528 To prepare samples for TEM, MCF10A cells expressing ER-FlucDM-eGFP were synchronized to the

529 G2/M boundary by treating cells with RO-3306 for 16 to 20 h and were released into mitosis by
530 removing RO-3306. After 45 min released from the G2/M boundary, cells were trypsinized for 10 min
531 before centrifugation. The cell pellet was fixed by 2.5% paraformaldehyde (in PBS) for 30 min at
532 room temperature before overnight at 4°C. Fixed pellet was further fixed by 1% osmium tetroxide
533 and then 2% uranium acetate. Ethanol and acetone were used to dehydrate samples before
534 embedding them into epoxy resin. Sectioned samples were observed by Tecnai G2 spirit 120kV
535 transmission electron microscopy (Thermo FEI).
536
537 **Live-cell staining**
538 The live-cell staining dyes used are as follow: 100 nM SiR-Tubulin (Cytoskeleton, CY-SC002), 1 μM
539 ER-tracker Red (Beyotime, C1041S) or 10 μM Thioflavin T (ThT) in the medium to label cells for
540 about 30 min in the incubator before imaging. For ThT staining, about ten percent aggregates could
541 be stained by ThT in ER-FlucDM-mCherry cells.
542
543 **Spinning-disk confocal microscopy imaging**
544 The hardware configuration of the spinning-disk confocal microscopy system was as described
545 previously (Wang et al., 2023). Imaging utilized a z-step size of 0.5 μm, with a x-y plane resolution
546 of 183.3 nm/pixel for the 60× lens and 110 nm/pixel for the 100× lens. Fluorophores were excited
547 using laser lines at wavelengths of 405, 488, 561, or 640 nm.
548
549 For FRAP analysis, images were acquired with 488 nm and 561 nm laser lines through the 100×
550 lens. The procedure involved acquiring three pre-bleach images every 30 seconds, followed by

551 bleaching the mCherry signal using the 561 nm laser. Subsequently, one image was acquired
552 immediately post-bleaching, followed by ten images acquired every 30 seconds. In total, fourteen
553 time-point images were acquired, and the total duration of each FRAP experiment was 6.5 minutes.
554

555 **Image analysis and processing**

556 Fiji was used to process images. Z-stack images for quantification were first projected using max-
557 intensity projection (Fiji/image/stacks/Z project). To quantify aggregates, projected images were
558 classified by Trainable Weka Segmentation (Fiji/Plugins/Segmentation/Trainable Weka
559 Segmentation). The segmented images were processed by using the ImageJ Macro commands:
560 run("8-bit"); setOption("BlackBackground", true); run("Convert to Mask"); run("Watershed") before
561 using Analyze Particles (Fiji/Analyze/Analyze Particles). For time-lapse images except images from
562 FRAP, the segmented images were processed by using the ImageJ Macro commands: run("8-bit");
563 setThreshold(0, 120); run("Make Binary", "method=Default background=Light black"); run("Invert
564 LUT"); run("Watershed", "stack") before using Analyze Particles (Fiji/Analyze/Analyze Particles).
565

566 To quantify total GFP intensities in live cells, Z-stack images (24 μm) were acquired and projected
567 using sum slices projection. Cell outlines were segmented using polygon selection in Fiji. To
568 quantitate the background intensity, the mean intensity of a small dark region of the field-of-view was
569 measured and multiplied by the area of the segmented cell. The background was subtracted from
570 the GFP intensity of segmented cells.
571

572 For FRAP analysis of ER-eGFP and ER-HaloDM-eGFP, region-of-interests (ROI) in projected

images were manually selected and the average fluorescence intensity of ROIs was measured in Fiji. For FRAP analysis of aggregates in cells co-expressing ER-FlucDM-eGFP and ER-FlucDM-mCherry (both interphase and mitosis), the aggregates were first segmented by Weka Segmentation. The unsegmented images from the mCherry channel were processed by Analyze Particles (Fiji/Analyze/Analyze Particles) based on the corresponding segmented images from the GFP channel. For fluorescence intensity quantification, background in all FRAP experiments were subtracted by one hundreds.

**Quantification and statistical analysis**

Datasets were analysed by Student's t test or Mann-Whitney test. Prism 8 (GraphPad) was used for the statistical analysis and data plotting. Statistical details are indicated in the figure legends.

**Author contributions**

S.D conceived the study, designed and performed experiments, and analyzed data. Y.W, B.C, S.X, K.Y.C provided some reagents used in the study. D.H participated in the discussion during project development. T.G.C. conceived the study, designed experiments and supervised the study. D.S and T.G.C prepared the manuscript with inputs from D.H.

**Acknowledgements**

This study was funded by National Natural Science Foundation of China (NSFC) RFIS-II grant (32350610247) and NFSC grant (32270770) given to T.G.C. We thank Xiaoxia Wan and Chenyu Yang in the Center of Cryo-Electron Microscopy (CCEM), Zhejiang University for their technical

595 assistance on Transmission Electron Microscopy. We thank Xuqi Chen, Xukai Gao and Zihan Chu
596 for participating in the early stage of the project. We thank Dr. Mike Shipston for participating in the
597 discussion. We thank all lab members for discussion.

598

599 **Conflict of interest**

600 The authors declare that they have no conflict of interest.

601

602 **Figure legends**

603 **Figure 1. ER-FlucDM-eGFP forms protein aggregates in the nucleus.**

604 (A) Representative images of ER-FlucDM-eGFP expressed in different cell lines. Maximum
605 projected images were shown.

606 (B) Microscopy images of cells expressing ER-FlucDM-mCherry and mStayGold-Sec61β. Single Z-
607 slice images were shown.

608 (C) Quantification of the luciferase activity in MCF10A cells expressing different constructs. Unpaired
609 t-test. Data were collected from three independent experiments. Abundance of GFP fusion
610 proteins was determined using protein blotting and was used in normalization.

611 (D) Representative images to show MCF10A cells expressing ER-FlucDM-mCherry, $ER^{FSHR}$-
612 FlucDM-eGFP (signal peptide sequence from the N-terminus of FSHR), ER-HaloDM-eGFP or
613 ER-eGFP. Maximum projected images were shown.

614 (E) Images of ER-FlucDM-eGFP aggregates surrounded by the ER membrane in a MCF10A cell.
615 Single Z-slice images were shown.

616 (F) TEM images of sectioned MCF10A interphase cells expressing ER-FlucDM-eGFP.

617 Data represent mean + SD. Scale bar, 10 μm (A to E).

618

619 **Figure 2. Differential aggregate dynamics in cells at interphase and mitosis.**

620 (A) Representative images of interphase cells co-expressing ER-FlucDM-eGFP and ER-FlucDM-
621 mCherry before and after photobleaching. Yellow rectangles indicate bleached aggregates.
622 Maximum projected images were shown.

623 (B) Representative images of mitotic cells co-expressing ER-FlucDM-eGFP and ER-FlucDM-
624 mCherry before and after photobleaching. Yellow circles indicate bleached aggregates.
625 Maximum projected images were shown.

626 (C) Recovery curves of ER-FlucDM-mCherry intensity after photobleaching. 14 ROIs from the ER of
627 interphase cells, 14 aggregates from mitotic cells, 26 aggregates from interphase cells. Data
628 represent mean + SD. A small region of ER-FlucDM-mCherry in the ER network was chosen as
629 a control for photobleaching.

630 (D) Quantification of the ER-FlucDM-mCherry intensity of bleached aggregates right after bleaching
631 and after 5 min of recovery. 0 min and 5 min refer to the time points in (C). Paired t-test (two-
632 tailed).

633 Data were collected from four independent experiments. Scale bar, 10 μm.

634

635 **Figure 3. Aggregates are cleared during cell division.**

636 (A) Representative images of dividing ER-FlucDM-eGFP cells at different cell cycle phases. Grey
637 scale bar: telophase and early G1 cells; black scale bar: interphase and prophase, prometaphase,
638 metaphase, anaphase. Maximum projected images were shown. Scale bar, 10 μm.

639 (B) Quantification of ER-FlucDM-eGFP aggregates from dividing cells. Count and area are individual
640 cell data. Each grey ring represents aggregates from one cell. Interphase and prophase, 91 cells;
641 prometaphase, 45 cells; metaphase, 60 cells; anaphase, 20 cells; telophase and early G1, 73
642 cells. From three independent experiments. Unpaired two side Mann-Whitney U-test. Data
643 represent mean ± SD
644 (C) Representative time-lapse images of cells expressing ER-FlucDM-eGFP released from the G2/M
645 boundary. NEB (nuclear envelop breakdown) is set to be t = 0 min. Maximum projected images
646 were shown. Scale bar, 10 μm.
647 (D) Quantification of aggregate number and area of dividing cells expressing ER-FlucDM-eGFP. Left
648 panel: data of individual cells. Right panel: mean values + SD of single-cell data (left panel). Time
649 point of NEB in each cell was set to 0 min. Aggregate count and total area of each cell at each
650 time point is normalized to its own value at t = 0 min. Aggregate count data are from 61 interphase
651 and 73 dividing cells of four independent experiments. Aggregate area of each cell is calculated
652 from 32 interphase and 34 dividing cells of two independent experiments.
653
654
655 **Figure 4. Effects of ER stressors on aggregate clearance.**
656 (A) Relative gene expression levels of chaperones and co-chaperones in cells expressing ER-
657 FlucDM-eGFP. Four independent experiments.
658 (B) Images of cells treated with DMSO or 1 μM Thaps and fixed at 35 min or 65 min after released
659 from the G2/M boundary. Maximum projected images were shown.
660 (C) Quantification of cells treated with DMSO or 1 μM Thaps and fixed at 35 min or 65 min after

661 released from the G2/M boundary. 35 min_DMSO, 207 cells; 35 min_Thaps, 173 cells;
662 65min_DMSO, 244 cells; 65 min_Thaps, 209 cells. Unpaired two side Mann-Whitney U-test. The
663 solid black line in violin plot indicates median of data in the column. Gray dotted lines are quartiles.
664 Each light pink circle indicates measurements of individual cells.
665 (D) Representative time-lapse images of cells expressing ER-FlucDM-eGFP treated with DMSO or
666 1 μM Thaps after released from the G2/M boundary. Maximum projected images were shown.
667 (E) Quantification of cells expressing ER-FlucDM-eGFP treated with DMSO or 1 μM Thaps. Time
668 point of NEB in each cell was set to 0 min. Aggregates count and total area of each cell is
669 normalized to its own value at t = 0 min. Black dotted lines are 90 min since NEB. DMSO, 89
670 cells; Thaps, 65 cells.
671 Scale bar, 10 μm. Three (C and E) or four (A) independent experiments.
672
673 **Figure 5. Inhibition of HSP70 and BiP prevents aggregate clearance.**
674 (A) Representative images of cells expressing ER-FlucDM-eGFP treated with DMSO or 50 μM VER
675 and fixed at 65 min after released from the G2/M boundary. Maximum projected images were
676 shown.
677 (B) Quantification of cells expressing ER-FlucDM-eGFP treated with DMSO or 50 μM VER and fixed
678 at 65 min after released from the G2/M boundary. DMSO, 357 cells; VER, 465 cells.
679 (C) Time-lapse images of dividing cells expressing ER-FlucDM-eGFP treated with DMSO or 50 μM
680 VER. Maximum projected images were shown.
681 (D) Representative images of cells expressing ER-FlucDM-eGFP treated with DMSO or different
682 concentrations of YUM70. Maximum projected images were shown.

683 (E) Quantification of cells expressing ER-FlucDM-eGFP treated with DMSO or YUM70 and fixed at
684 65 min after released from the G2/M boundary. DMSO, 310 cells; 5 μM YUM70, 258 cells; 20 μM
685 YUM70, 215 cells; 50 μM YUM70, 209 cells; 100 μM YUM70, 287 cells.
686 Scale bar, 10 μm. Unpaired two side Mann-Whitney U-test. Each solid line in violin plot indicates
687 median of data in the column. Gray dotted lines are quartiles. A, B, D and E are from three
688 independent experiments. C is from two independent experiments
689
690 **Figure 6. Effects of MG132, APCi and RO-3306 (Cdk1i) on aggregate clearance.**
691 (A) Representative images of cells expressing ER-FlucDM-eGFP arrested at mitosis by MG132 and
692 further treated with Cdk1i to induce mitotic exit. Cells were first treated with 25 μM MG132 for 55
693 min and mitotic arrested cells were further treated with 25 μM MG132 plus 10 μM RO-3306 or
694 25 μM MG132 only. Cells were fixed 40 min after the second treatment. Maximum projected
695 images were shown.
696 (B) Quantification of (A). MG132 only, 442 cells; MG132 + RO-3306, 374 cells.
697 (C) Time-lapse images of cells expressing ER-FlucDM-eGFP arrested at mitosis by MG132 and
698 further treated with RO-3306 to induce mitotic exit. Cells were treated with 25 μM MG132 for 55
699 min, and further treated with 25 μM MG132 plus 10 μM RO-3306 or 25 μM MG132 before imaging.
700 Maximum projected images were shown.
701 (D) Quantification of (C). Remaining aggregates at 40 min were calculated for their aggregates count
702 or area and compared to that of in 0 min. MG132 only, 125 cells; MG132 + RO-3306, 134 cells.
703 (E) Images of cells expressing ER-FlucDM-eGFP treated with DMSO or APCi (20 μM proTAME and
704 300 μM Apcin) and fixed at 55 min after released from the G2/M boundary. Maximum projected

705 images were shown.

706 (F) Quantifications of cells expressing ER-FlucDM-eGFP treated with DMSO or APCi (20 μM
707 proTAME and 300 μM Apcin). DMSO, 450 cells; APCi, 549 cells.

708 (G) Images of cells at telophase or cells of newly divided upon treatment of DMSO or APCi for 35 to
709 40 min. Maximum projected images were shown.

710 (H) Cells at telophase or newly divided cells that have aggregates upon treatment of DMSO or APCi
711 were counted.

712 (I) Aggregates number and area were counted in cells at telophase or in newly divided cells after
713 treated with DMSO or APCi. Only cells with aggregates were included in the quantification.
714 DMSO, 297 cells; APCi, 319 cells.

715 Scale bar, 10 μm. Data are from at least three independent experiments and analysed by unpaired
716 two side Mann-Whitney U-test (B, D, F and I) or paired t-test (H).

717

718 **Figure 7. Perturbation of proteins that regulate ER reorganization in aggregate clearance**

719 (A) Images of cells expressing ER-FlucDM-eGFP after depletion of Atlastin 2 and Atlastin 3 and fixed
720 at 65 min after released from the G2/M boundary. Maximum projected images were shown.

721 (B) Quantification of cells expressing ER-FlucDM-eGFP after depletion of Atlastin 2 and Atlastin 3
722 and fixed at 65 min after released from the G2/M boundary. Control, 396 cells; ATL2/ATL3 KD,
723 362 cells.

724 (C) Images of cells expressing ER-FlucDM-eGFP treated with DMSO or 100 nM MLN-8237 and fixed
725 at 65 min after released from the G2/M boundary. Maximum projected images were shown.

726 (D) Quantification of cells expressing ER-FlucDM-eGFP treated with DMSO or 100 nM MLN-8237

727 and fixed at 65 min after released from the G2/M boundary. Only round mitotic cells were counted.
728 DMSO, 102 cells; MLN-8237, 288 cells.
729 (E) Images of cells expressing ER-FlucDM-eGFP treated with DMSO or 331nM nocodazole and
730 fixed at 65 min after released from the G2/M boundary. Maximum projected images were shown.
731 (F) Quantification of cells expressing ER-FlucDM-eGFP treated with DMSO or 331nM nocodazole
732 and fixed at 65 min after released from the G2/M boundary. Only round mitotic cells were counted.
733 DMSO, 122 cells; nocodazole, 320 cells.
734 Scale bar, 10 μm. Data are from three independent experiments and analysed by unpaired two side
735 Mann-Whitney U-test.
736
737 **Supplementary figures**
738 **Figure S1. ER-FlucDM-eGFP forms protein aggregates, related to Figure 1**
739 (A) Microscopy images of cells expressing NLS-FlucDM-eGFP. Two cell lines were used to express
740 NLS-FlucDM-eGFP. Single Z-slice images were shown.
741 (B) Microscopy images of cells expressing NLS-FlucDM-eGFP and ER-FlucDM-mCherry in MCF10A
742 cells. Single Z-slice images were shown.
743 (C) Protein blots for ER-FlucDM-eGFP and NLS-FlucDM-eGFP using anti-GFP or anti-β-actin
744 antibodies.
745 (D) Relative GFP protein intensity in S1(C) was quantitated and plotted. The intensity of β-actin was
746 used in normalization.
747 (E) Protein blotting to examine solubility of ER-FlucDM-eGFP under different concentrations of
748 detergents, NP-40. Cells expressing ER-FlucDM-eGFP were subjected to 45 °C for 1 hour before

749 harvesting cell lysates in heat shock experiments. Insoluble fractions were quantitated and
750 plotted.
751 (F) Colocalization of ER-FlucDM-eGFP and Thioflavin T (ThT), a marker for protein aggregates.
752 Single Z-slice images were shown.
753 (G) Quantification of ER-FlucDM-eGFP aggregate number (left) and total aggregate area (right) of
754 individual cells in different cell lines. MCF10A, 516 cells; A549, 395 cells; MDA-MB-231, 369
755 cells; U2OS, 528 cells.
756 (H) Schematic representation of different constructs used in this study.
757 (I) Quantification of aggregate number in cells expressing ER-eGFP, ER-HaloWT-eGFP, ER-
758 HaloDM-eGFP. ER-eGFP, 612 cells; ER-HaloWT-eGFP, 405 cells; 546 ER-HaloDM-eGFP, 546
759 cells; ER-FlucDM-eGFP, 516 cells.
760 Data are from three independent experiments, analysed by unpaired t-test and represented by mean
761 + SD. Scale bar, 10 μm.
762
763 **Figure S2. FRAP analysis of protein aggregates, related to Figure 2.**
764 (A) Recovery curve of ER-HaloDM-eGFP before and after photobleaching. Seven interphase cells
765 from three independent experiments. Data represent mean + SD.
766 (B) Recovery curve of individual cell data in ER-FlucDM-eGFP before and after photobleaching. 14
767 ROIs from the ER of interphase cell, 14 aggregates from cells at mitosis, 26 aggregates from
768 cells at interphase. Data were collected from four independent experiments.
769 (C) Recovery curve of ER-eGFP before and after photobleaching. Seven interphase cells from three
770 independent experiments. Data represent mean + SD.

771 (D) Quantification of protein fluorescence intensity of different constructs right after photobleaching
772 and 5 min after recovery. 0 min is the protein intensity right after photobleaching and 5 min is the
773 protein intensity 5 min after recovery from photobleaching. At least three independent
774 experiments. Data represent mean ± SD.
775
776 **Figure S3. Aggregates in dividing cells, related to Figure 3.**
777 (A) Images to show ER-FlucDM-eGFP aggregates of dividing cells were surrounded by the
778 membrane stained by the ER-tracker. Scale bar, 10 μm. Single Z-slice images were shown.
779 (B) TEM images of sectioned MCF10A mitotic cells expressing ER-FlucDM-eGFP.
780 (C) Time-lapse images of cells expressing ER-HaloDM-eGFP released from the G2/M boundary.
781 NEB (nuclear envelop breakdown) is set to be t = 0 min. Maximum projected images were shown.
782 Scale bar, 10 μm.
783 (D) Linear regression analysis to show that cell division process is not linearly dependent on
784 aggregates quantity. 74 dividing cells are from four independent experiments.
785
786 **Figure S4. Effect of Thapsigargin or Tunicamycin on aggregates clearance, related to Figure**
787 **4.**
788 (A) Proteomic analysis of cells expressing ER-FlucDM-eGFP. Three independent experiments.
789 Proteins involved in ER stress and unfolded protein response (blue) or cell cycle and cell division
790 (pink) were highlighted.
791 (B) Changes of aggregate number and total area as a function of time after cells expressing ER-
792 FlucDM-eGFP were treated with DMSO or 1 μM Thaps.

793 (C) Quantification of aggregate number and total area of cells expressing ER-FlucDM-eGFP treated
794 with DMSO or Tunicamycin (Tuni) during mitosis. DMSO, 542 cells; 200 ng/mL Tuni, 385 cells;
795 2 μg/mL Tuni, 471 cells; 10 μg/mL Tuni, 439 cells. Four independent experiments. Unpaired two
796 side Mann-Whitney U-test. Each solid thick line in violin plot indicates median of data in the
797 column. Gray lines are quartiles.
798
799 **Figure S5. Colocalization of BiP and ER-FlucDM-eGFP, related to Figure 5.**
800 (A) Immunofluorescence staining of BiP and ER-FlucDM-eGFP in dividing cells. Maximum projected
801 images were shown.
802 (B) Colocalization analysis of BiP and ER-FlucDM-eGFP. R represents Pearson correlation
803 coefficient (r).
804 (C) Immunofluorescence staining of BiP and ER-FlucDM-eGFP in interphase cells. Single Z-slice
805 images were shown.
806 Scale bar, 10 μm. Three independent experiments.
807
808 **Figure S6. MG132, APCi and RO-3306 treatments on aggregate clearance, related to Figure 6.**
809 (A) Quantification of the aggregate number in cells expressing ER-FlucDM-eGFP treated with DMSO
810 or 25 μM MG132 and fixed at 55 min after released from the G2/M boundary. DMSO, 293 cells;
811 MG132, 350 cells. Maximum projected images were shown.
812 (B) Quantification of the aggregate number in cells expressing ER-FlucDM-eGFP treated with DMSO
813 or 5 μM MG132 and fixed at 55 min since release. DMSO, 295 cells; MG132, 436 cells. Maximum
814 projected images were shown.

815 (C) Images of cells at telophase or newly divided cells after treated with DMSO or 25 μM MG132 for
816 35 min. Maximum projected images were shown.
817 (D) Cells at telophase or newly divided cells that have aggregates upon treatment of 25 μM MG132
818 were counted. DMSO, 455 cells; MG132, 393 cells.
819 (E) Aggregates number and area were counted in cells at telophase or in newly divided cells after
820 treated with DMSO or 25 μM MG132. Only cells with aggregates were included in the
821 quantification. DMSO, 294 cells; MG132, 339 cells.
822 (F) Images of cells at telophase and newly divided cells after treated with DMSO or 5 μM MG132 for
823 35 min. Maximum projected images were shown.
824 (G) Cells at telophase or newly divided cells that have aggregates upon treatment of DMSO or 5 μM
825 MG132. DMSO, 676 cells; APCi, 646 cells.
826 (H) Aggregates number and area were counted in cells at telophase or in newly divided cells after
827 treated with DMSO or 5 μM MG132. Only cells with aggregates were included in the
828 quantification. DMSO, 227 cells; MG132, 297 cells.
829 (I) Quantification of the aggregate number in cells expressing ER-FlucDM-eGFP treated with 5 μM
830 MG132 or 5 μM MG132 + RO-3306.
831 (J) Images of cells co-expressing ER-FlucDM-mCherry and mGreenLantern-hGeminin (degron).
832 Left panel: cells were treated with DMSO or APC/Ci after 65 min released from the G2/M. Right
833 panel: after 65 min released from the G2/M, cells were treated with DMSO or APC/Ci for 40
834 minutes using live-cell imaging. Maximum projected images were shown.
835 (K) Quantification of mGreenLantern-hGeminin (degron) intensity of cells treated with DMSO or
836 APC/Ci for 40 min.

837 Scale bar, 10 μm. Data are from at least three independent experiments and analysed by unpaired
838 two side Mann-Whitney U-test (A, B, E, H and I), unpaired t-test (K) and paired t-test (D and G).
839
840 **Figure S7. Cycloheximide chase experiment and microscopy quantification of cells**
841 **expressing ER-FlucDM-eGFP, related to Figure 6.**
842 (A) Protein blots of ER-FlucDM-eGFP, Cyclin B1, p53 and β-actin under DMSO or 200 μM CHX
843 treatments. Cells were synchronized to the G2/M boundary and released into medium containing
844 DMSO or CHX and lysates were harvested.
845 (B) Protein levels of p53 and Cyclin B1 in different time points after DMSO or CHX treatments were
846 measured and plotted. Levels of β-actin were used in normalization.
847 (C) Protein levels of ER-FlucDM-eGFP in different time points after DMSO or CHX treatments were
848 measured and plotted. Levels of β-actin were used in normalization.
849 (D) Relative intensity of ER-FlucDM-eGFP in early and late dividing cells.
850 Scale bar, 10 μm. Data are from three independent experiments and analysed by unpaired t-test.
851
852 **References**


853 Aguilaniu, H., L. Gustafsson, M. Rigoulet, and T. Nystrom. 2003. Asymmetric inheritance of oxidatively damaged
854 proteins during cytokinesis. *Science*. 299:1751-1753.
855 Ando, R., S. Shimozono, H. Ago, M. Takagi, M. Sugiyama, H. Kurokawa, M. Hirano, Y. Niino, G. Ueno, F. Ishidate, T.
856 Fujiwara, Y. Okada, M. Yamamoto, and A. Miyawaki. 2024. StayGold variants for molecular fusion and
857 membrane-targeting applications. *Nat Methods*. 21:648-656.
858 Balch, W.E., R.I. Morimoto, A. Dillin, and J.W. Kelly. 2008. Adapting proteostasis for disease intervention. *Science*.
859 319:916-919.
860 Becher, I., A. Andres-Pons, N. Romanov, F. Stein, M. Schramm, F. Baudin, D. Helm, N. Kurzawa, A. Mateus, M.T.
861 Mackmull, A. Typas, C.W. Muller, P. Bork, M. Beck, and M.M. Savitski. 2018. Pervasive Protein Thermal
862 Stability Variation during the Cell Cycle. *Cell*. 173:1495-1507 e1418.
863 Bergman, Z.J., J.D. McLaurin, A.S. Eritano, B.M. Johnson, A.Q. Sims, and B. Riggs. 2015. Spatial reorganization of
864 the endoplasmic reticulum during mitosis relies on mitotic kinase cyclin A in the early Drosophila embryo.
865 *PLoS One*. 10:e0117859.

866 Clay, L., F. Caudron, A. Denoth-Lippuner, B. Boettcher, S. Buvelot Frei, E.L. Snapp, and Y. Barral. 2014. A
867 sphingolipid-dependent diffusion barrier confines ER stress to the yeast mother cell. *Elife*. 3:e01883.
868 Dickens, J.A., A. Ordonez, J.E. Chambers, A.J. Beckett, V. Patel, E. Malzer, C.S. Dominicus, J. Bradley, A.A. Peden, I.A.
869 Prior, D.A. Lomas, and S.J. Marciniak. 2016. The endoplasmic reticulum remains functionally connected by
870 vesicular transport after its fragmentation in cells expressing Z-alpha1-antitrypsin. *FASEB J*. 30:4083-4097.
871 Fuentealba, L.C., E. Eivers, D. Geissert, V. Taelman, and E.M. De Robertis. 2008. Asymmetric mitosis: Unequal
872 segregation of proteins destined for degradation. *Proc Natl Acad Sci U S A*. 105:7732-7737.
873 Ghislain, M., A. Udvardy, and C. Mann. 1993. S. cerevisiae 26S protease mutants arrest cell division in
874 G2/metaphase. *Nature*. 366:358-362.
875 Glotzer, M., A.W. Murray, and M.W. Kirschner. 1991. Cyclin is degraded by the ubiquitin pathway. *Nature*. 349:132-
876 138.
877 Gupta, R., P. Kasturi, A. Bracher, C. Loew, M. Zheng, A. Villella, D. Garza, F.U. Hartl, and S. Raychaudhuri. 2011.
878 Firefly luciferase mutants as sensors of proteome stress. *Nat Methods*. 8:879-884.
879 Hartl, F.U., A. Bracher, and M. Hayer-Hartl. 2011. Molecular chaperones in protein folding and proteostasis. *Nature*.
880 475:324-332.
881 Hill, S.M., S. Hanzen, and T. Nystrom. 2017. Restricted access: spatial sequestration of damaged proteins during
882 stress and aging. *EMBO Rep*. 18:377-391.
883 Hipp, M.S., P. Kasturi, and F.U. Hartl. 2019. The proteostasis network and its decline in ageing. *Nat Rev Mol Cell*
884 *Biol*. 20:421-435.
885 Jayaraj, G.G., M.S. Hipp, and F.U. Hartl. 2020. Functional Modules of the Proteostasis Network. *Cold Spring Harb*
886 *Perspect Biol*. 12.
887 Kaganovich, D., R. Kopito, and J. Frydman. 2008. Misfolded proteins partition between two distinct quality control
888 compartments. *Nature*. 454:1088-1095.
889 Kakihana, A., Y. Oto, Y. Saito, and Y. Nakayama. 2019. Heat shock-induced mitotic arrest requires heat shock
890 protein 105 for the activation of spindle assembly checkpoint. *FASEB J*. 33:3936-3953.
891 Labbadia, J., and R.I. Morimoto. 2015. The biology of proteostasis in aging and disease. *Annu Rev Biochem*.
892 84:435-464.
893 Lee, C., M. Ferguson, and L.B. Chen. 1989. Construction of the endoplasmic reticulum. *J Cell Biol*. 109:2045-2055.
894 Liu, Z., G. Liu, D.P. Ha, J. Wang, M. Xiong, and A.S. Lee. 2023. ER chaperone GRP78/BiP translocates to the nucleus
895 under stress and acts as a transcriptional regulator. *Proc Natl Acad Sci U S A*. 120:e2303448120.
896 Melo, E.P., T. Konno, I. Farace, M.A. Awadelkareem, L.R. Skov, F. Teodoro, T.P. Sancho, A.W. Paton, J.C. Paton, M.
897 Fares, P.M.R. Paulo, X. Zhang, and E. Avezov. 2022. Stress-induced protein disaggregation in the
898 endoplasmic reticulum catalysed by BiP. *Nat Commun*. 13:2501.
899 Miyata, T., D. Hagiwara, Y. Hodai, T. Miwata, Y. Kawaguchi, J. Kurimoto, H. Ozaki, K. Mitsumoto, H. Takagi, H. Suga,
900 T. Kobayashi, M. Sugiyama, T. Onoue, Y. Ito, S. Iwama, R. Banno, M. Matsumoto, N. Kawakami, N. Ohno,
901 H. Sakamoto, and H. Arima. 2020. Degradation of Mutant Protein Aggregates within the Endoplasmic
902 Reticulum of Vasopressin Neurons. *iScience*. 23:101648.
903 Mochida, K., and H. Nakatogawa. 2022. ER-phagy: selective autophagy of the endoplasmic reticulum. *EMBO Rep*.
904 23:e55192.
905 Morris, J.A., A.J. Dorner, C.A. Edwards, L.M. Hendershot, and R.J. Kaufman. 1997. Immunoglobulin binding protein
906 (BiP) function is required to protect cells from endoplasmic reticulum stress but is not required for the
907 secretion of selective proteins. *J Biol Chem*. 272:4327-4334.
908 Nillegoda, N.B., J. Kirstein, A. Szlachcic, M. Berynskyy, A. Stank, F. Stengel, K. Arnsburg, X. Gao, A. Scior, R. Aebersold,
909 D.L. Guilbride, R.C. Wade, R.I. Morimoto, M.P. Mayer, and B. Bukau. 2015. Crucial HSP70 co-chaperone
910 complex unlocks metazoan protein disaggregation. *Nature*. 524:247-251.

Olzmann, J.A., R.R. Kopito, and J.C. Christianson. 2013. The mammalian endoplasmic reticulum-associated degradation system. *Cold Spring Harb Perspect Biol*. 5.

Olzscha, H., S.M. Schermann, A.C. Woerner, S. Pinkert, M.H. Hecht, G.G. Tartaglia, M. Vendruscolo, M. Hayer-Hartl, F.U. Hartl, and R.M. Vabulas. 2011. Amyloid-like aggregates sequester numerous metastable proteins with essential cellular functions. *Cell*. 144:67-78.

Palozola, K.C., G. Donahue, H. Liu, G.R. Grant, J.S. Becker, A. Cote, H. Yu, A. Raj, and K.S. Zaret. 2017. Mitotic transcription and waves of gene reactivation during mitotic exit. *Science*. 358:119-122.

Parashar, S., R. Chidambaram, S. Chen, C.R. Liem, E. Griffis, G.G. Lambert, N.C. Shaner, M. Wortham, J.C. Hay, and S. Ferro-Novick. 2021. Endoplasmic reticulum tubules limit the size of misfolded protein condensates. *Elife*. 10.

Pina, F.J., and M. Niwa. 2015. The ER Stress Surveillance (ERSU) pathway regulates daughter cell ER protein aggregate inheritance. *Elife*. 4.

Preissler, S., and D. Ron. 2019. Early Events in the Endoplasmic Reticulum Unfolded Protein Response. *Cold Spring Harb Perspect Biol*. 11.

Rosenzweig, R., N.B. Nillegoda, M.P. Mayer, and B. Bukau. 2019. The Hsp70 chaperone network. *Nat Rev Mol Cell Biol*. 20:665-680.

Rousseau, E., B. Dehay, L. Ben-Haiem, Y. Trottier, M. Morange, and A. Bertolotti. 2004. Targeting expression of expanded polyglutamine proteins to the endoplasmic reticulum or mitochondria prevents their aggregation. *Proc Natl Acad Sci U S A*. 101:9648-9653.

Rujano, M.A., F. Bosveld, F.A. Salomons, F. Dijk, M.A. van Waarde, J.J. van der Want, R.A. de Vos, E.R. Brunt, O.C. Sibon, and H.H. Kampinga. 2006. Polarised asymmetric inheritance of accumulated protein damage in higher eukaryotes. *PLoS Biol*. 4:e417.

Sackton, K.L., N. Dimova, X. Zeng, W. Tian, M. Zhang, T.B. Sackton, J. Meaders, K.L. Pfaff, F. Sigoillot, H. Yu, X. Luo, and R.W. King. 2014. Synergistic blockade of mitotic exit by two chemical inhibitors of the APC/C. *Nature*. 514:646-649.

Samanta, S., S. Yang, B. Debnath, D. Xue, Y. Kuang, K. Ramkumar, A.S. Lee, M. Ljungman, and N. Neamati. 2021. The Hydroxyquinoline Analogue YUM70 Inhibits GRP78 to Induce ER Stress-Mediated Apoptosis in Pancreatic Cancer. *Cancer Res*. 81:1883-1895.

Schlaitz, A.L., J. Thompson, C.C. Wong, J.R. Yates, 3rd, and R. Heald. 2013. REEP3/4 ensure endoplasmic reticulum clearance from metaphase chromatin and proper nuclear envelope architecture. *Dev Cell*. 26:315-323.

Sharma, R., M.M.D. Pramanik, B. Chandramouli, N. Rastogi, and N. Kumar. 2018. Understanding organellar protein folding capacities and assessing their pharmacological modulation by small molecules. *Eur J Cell Biol*. 97:114-125.

Shim, S.M., H.R. Choi, K.W. Sung, Y.J. Lee, S.T. Kim, D. Kim, S.R. Mun, J. Hwang, H. Cha-Molstad, A. Ciechanover, B.Y. Kim, and Y.T. Kwon. 2018. The endoplasmic reticulum-residing chaperone BiP is short-lived and metabolized through N-terminal arginylation. *Sci Signal*. 11.

Singhvi, A., and G. Garriga. 2009. Asymmetric divisions, aggresomes and apoptosis. *Trends Cell Biol*. 19:1-7.

Tyedmers, J., A. Mogk, and B. Bukau. 2010. Cellular strategies for controlling protein aggregation. *Nat Rev Mol Cell Biol*. 11:777-788.

Vincenz-Donnelly, L., H. Holthusen, R. Korner, E.C. Hansen, J. Presto, J. Johansson, R. Sawarkar, F.U. Hartl, and M.S. Hipp. 2018. High capacity of the endoplasmic reticulum to prevent secretion and aggregation of amyloidogenic proteins. *EMBO J*. 37:337-350.

Wang, C., J. Ding, Q. Wei, S. Du, X. Gong, and T.G. Chew. 2023. Mechanosensitive accumulation of non-muscle myosin IIB during mitosis requires its translocation activity. *iScience*. 26:107773.

Watson, E.R., N.G. Brown, J.M. Peters, H. Stark, and B.A. Schulman. 2019. Posing the APC/C E3 Ubiquitin Ligase to

Orchestrate Cell Division. *Trends Cell Biol*. 29:117-134.

Wirth, A.J., M. Platkov, and M. Gruebele. 2013. Temporal variation of a protein folding energy landscape in the cell. *J Am Chem Soc*. 135:19215-19221.

Wiseman, R.L., J.S. Mesgarzadeh, and L.M. Hendershot. 2022. Reshaping endoplasmic reticulum quality control through the unfolded protein response. *Mol Cell*. 82:1477-1491.

Woerner, A.C., F. Frottin, D. Hornburg, L.R. Feng, F. Meissner, M. Patra, J. Tatzelt, M. Mann, K.F. Winklhofer, F.U. Hartl, and M.S. Hipp. 2016. Cytoplasmic protein aggregates interfere with nucleocytoplasmic transport of protein and RNA. *Science*. 351:173-176.

Zhang, W., Z. Zhang, Y. Xiang, D.D. Gu, J. Chen, Y. Chen, S. Zhai, Y. Liu, T. Jiang, C. Liu, B. He, M. Yan, Z. Wang, J. Xu, Y.L. Cao, B. Deng, D. Zeng, J. Lei, J. Zhuo, X. Lei, Z. Long, B. Jin, T. Chen, D. Li, Y. Shen, J. Hu, S. Gao, and Q. Liu. 2024. Aurora kinase A-mediated phosphorylation triggers structural alteration of Rab1A to enhance ER complexity during mitosis. *Nat Struct Mol Biol*. 31:219-231.

Zhou, C., B.D. Slaughter, J.R. Unruh, F. Guo, Z. Yu, K. Mickey, A. Narkar, R.T. Ross, M. McClain, and R. Li. 2014. Organelle-based aggregation and retention of damaged proteins in asymmetrically dividing cells. *Cell*. 159:530-542.

# Figure 1

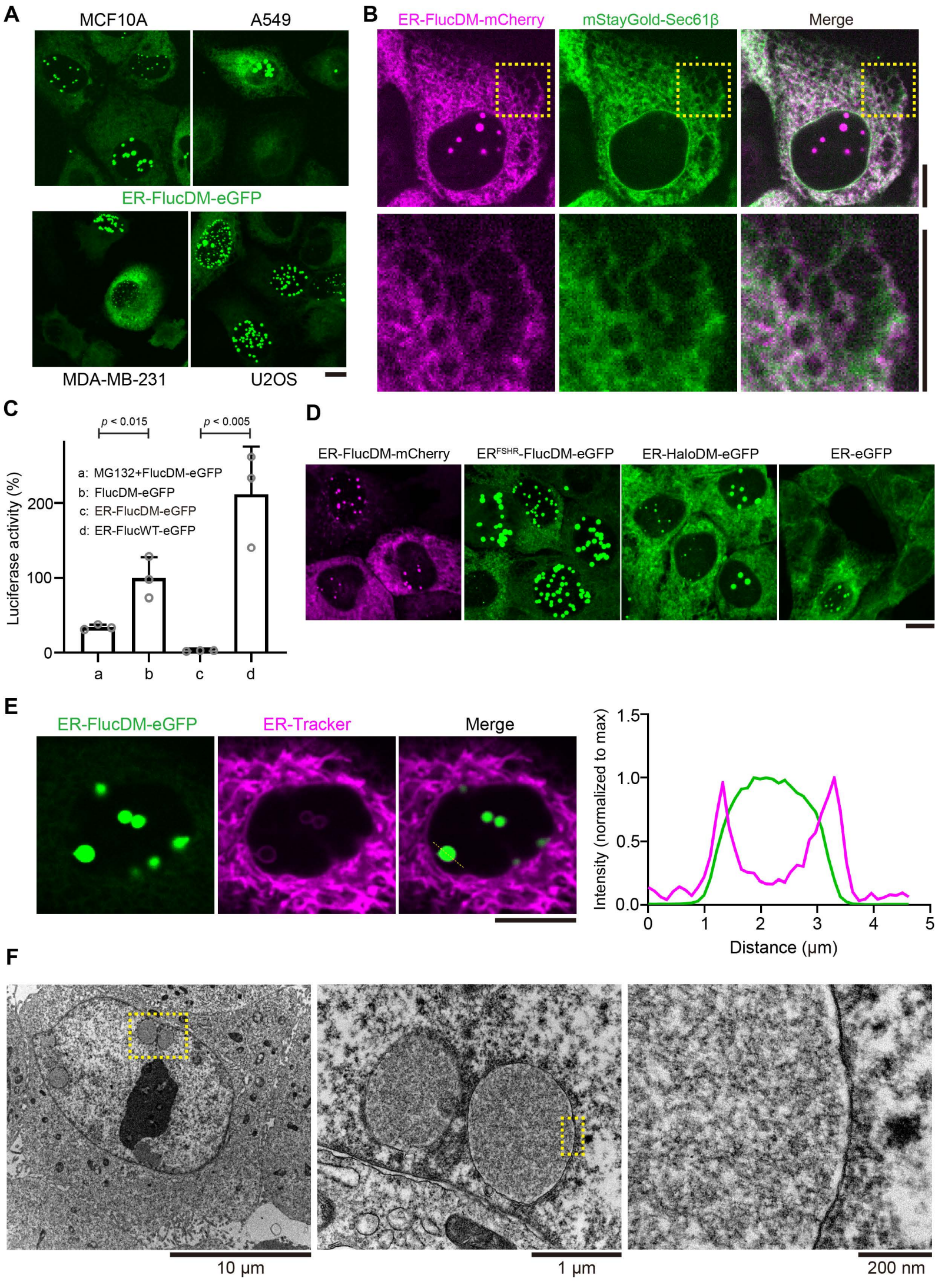
A
MCF10A
A549
ER-FlucDM-eGFP
MDA-MB-231
U2OS
B
ER-FlucDM-mCherry
mStayGold-Sec61β
Merge
C
p < 0.015
p < 0.005
a: MG132+FlucDM-eGFP
b: FlucDM-eGFP
c: ER-FlucDM-eGFP
d: ER-FlucWT-eGFP
Luciferase activity (%)
0
100
200
a
b
c
d
D
ER-FlucDM-mCherry
ERFSHR-FlucDM-eGFP
ER-HaloDM-eGFP
ER-eGFP
E
ER-FlucDM-eGFP
ER-Tracker
Merge
Intensity (normalized to max)
0.0
0.5
1.0
1.5
0
1
2
3
4
5
Distance (μm)
F
10 μm
1 μm
200 nm

# Figure 2

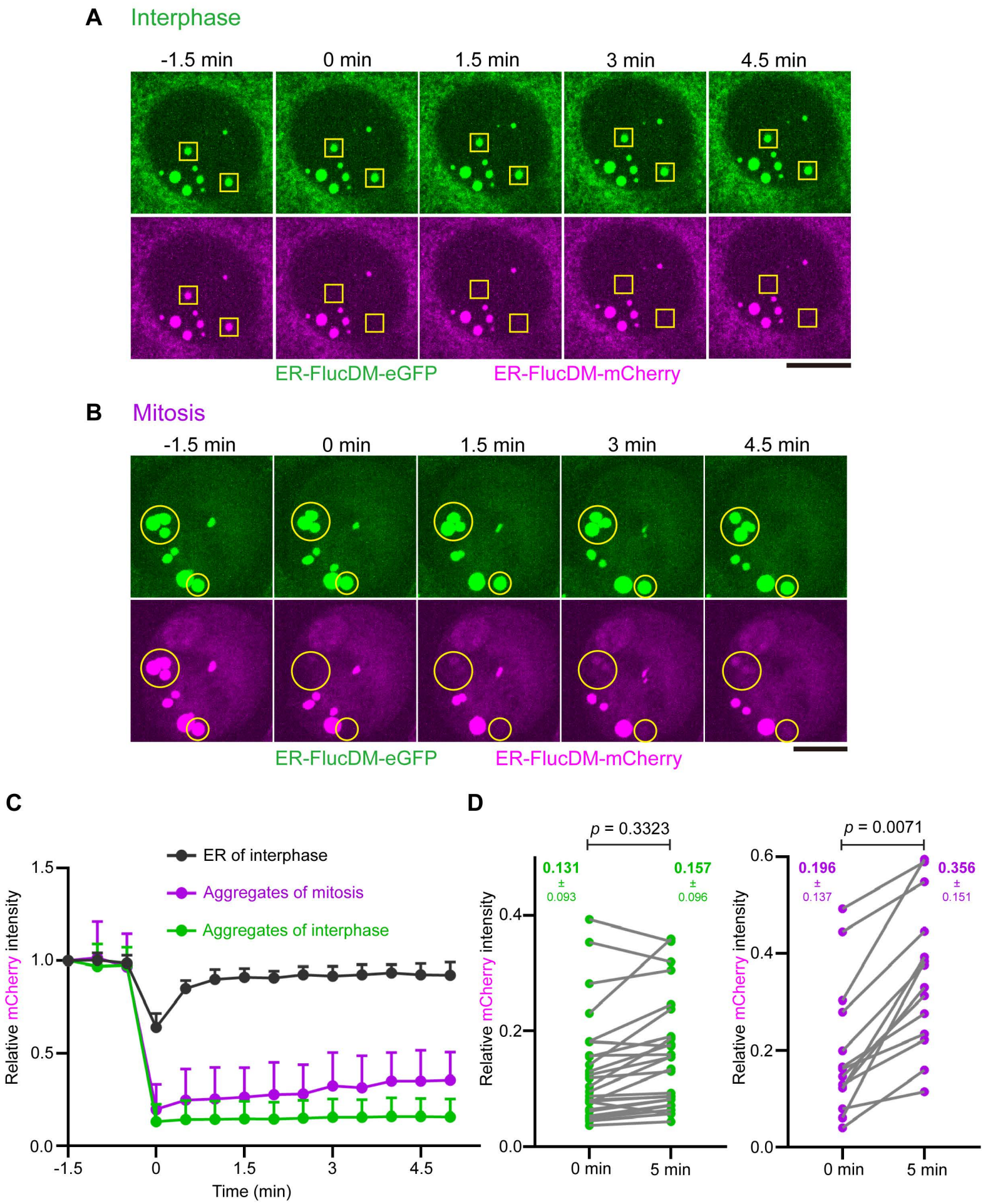
A
Interphase
-1.5 min
0 min
1.5 min
3 min
4.5 min
ER-FlucDM-eGFP
ER-FlucDM-mCherry
B
Mitosis
-1.5 min
0 min
1.5 min
3 min
4.5 min
ER-FlucDM-eGFP
ER-FlucDM-mCherry
C
ER of interphase
Aggregates of mitosis
Aggregates of interphase
Relative mCherry intensity
1.5
1.0
0.5
0.0
-1.5
0
1.5
3
4.5
Time (min)
D
p = 0.3323
0.131
±
0.093
0.157
±
0.096
Relative mCherry intensity
0.4
0.2
0.0
0 min
5 min
p = 0.0071
0.196
±
0.137
0.356
±
0.151
Relative mCherry intensity
0.6
0.4
0.2
0.0
0 min
5 min

# Figure 3

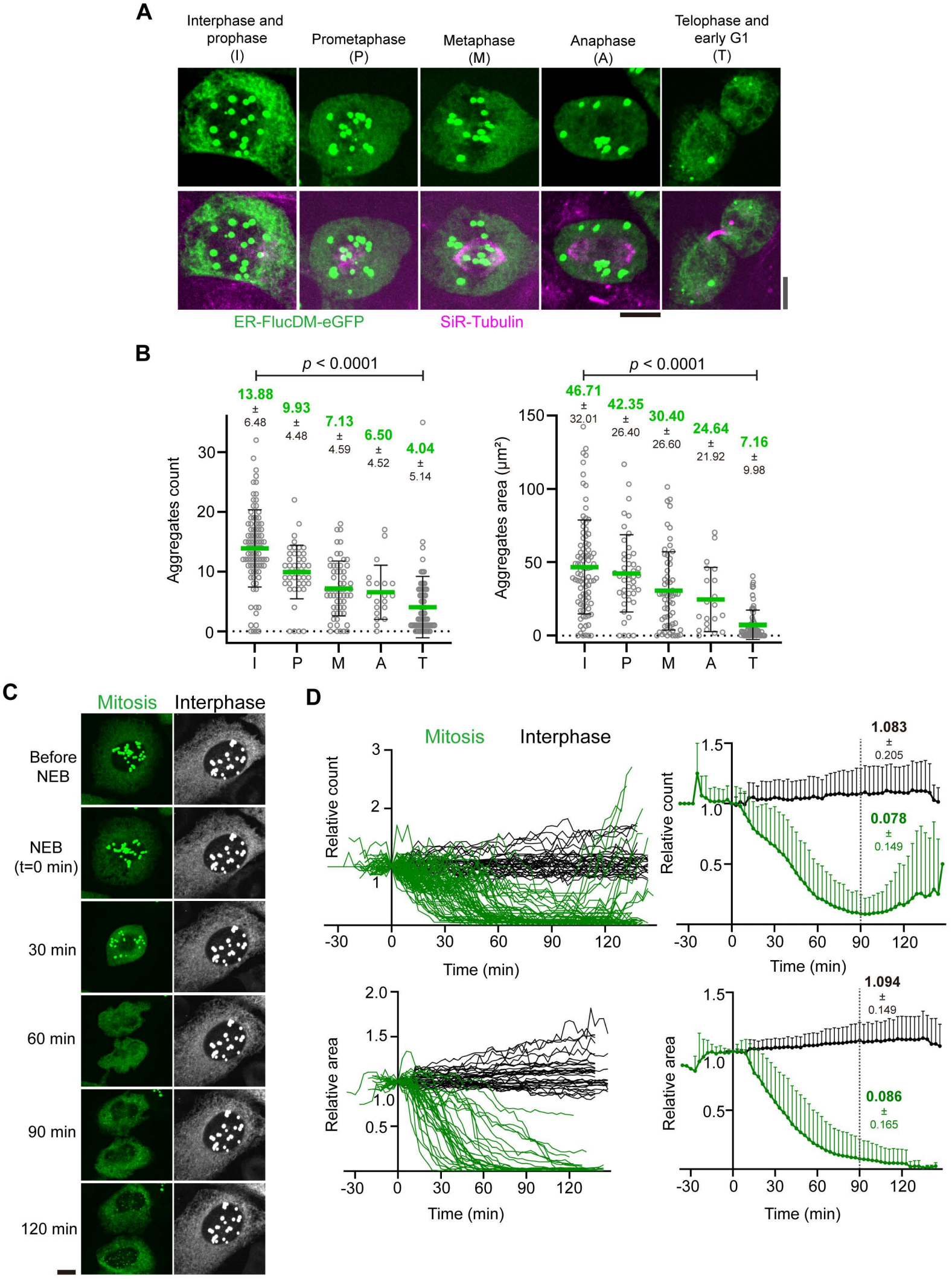
A
Interphase and prophase (I)
Prometaphase (P)
Metaphase (M)
Anaphase (A)
Telophase and early G1 (T)
ER-FlucDM-eGFP
SiR-Tubulin
B
p < 0.0001
Aggregates count
13.88 ± 6.48
9.93 ± 4.48
7.13 ± 4.59
6.50 ± 4.52
4.04 ± 5.14
I P M A T
p < 0.0001
Aggregates area (µm²)
46.71 ± 32.01
42.35 ± 26.40
30.40 ± 26.60
24.64 ± 21.92
7.16 ± 9.98
I P M A T
C
Mitosis
Interphase
Before NEB
NEB (t=0 min)
30 min
60 min
90 min
120 min
D
Mitosis
Interphase
Relative count
Time (min)
1.083 ± 0.205
0.078 ± 0.149
Relative area
1.094 ± 0.149
0.086 ± 0.165

# Figure 4

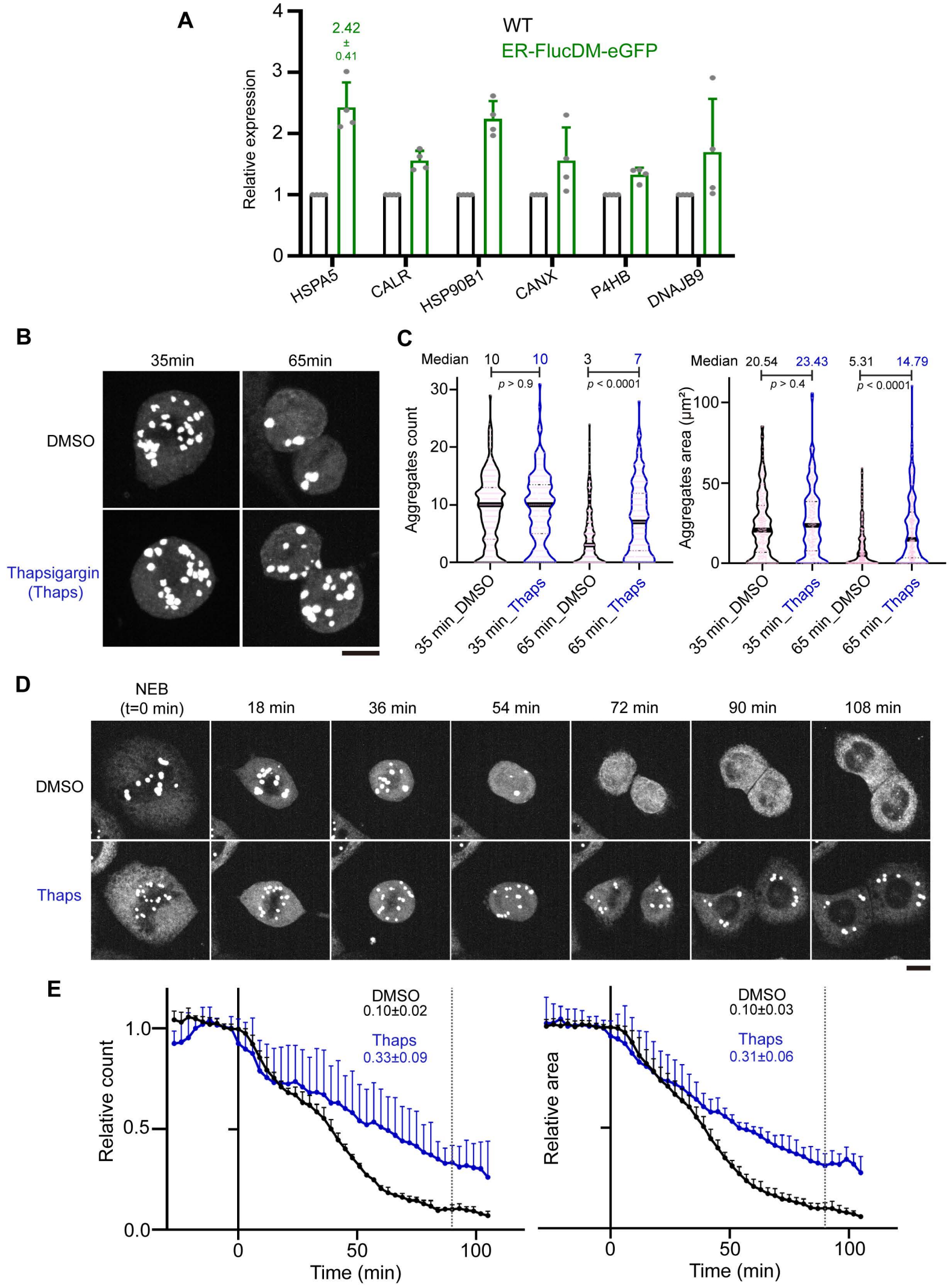
A
WT
ER-FlucDM-eGFP
2.42
±
0.41
Relative expression
HSPA5
CALR
HSP90B1
CANX
P4HB
DNAJB9
B
35min
65min
DMSO
Thapsigargin
(Thaps)
C
Median 10 10 3 7
p > 0.9
p < 0.0001
Aggregates count
Median 20.54 23.43 5.31 14.79
p > 0.4
p < 0.0001
Aggregates area (µm²)
35 min_DMSO
35 min_Thaps
65 min_DMSO
65 min_Thaps
D
NEB
(t=0 min)
18 min
36 min
54 min
72 min
90 min
108 min
DMSO
Thaps
E
DMSO
0.10±0.02
Thaps
0.33±0.09
Relative count
DMSO
0.10±0.03
Thaps
0.31±0.06
Relative area
Time (min)

# Figure 5

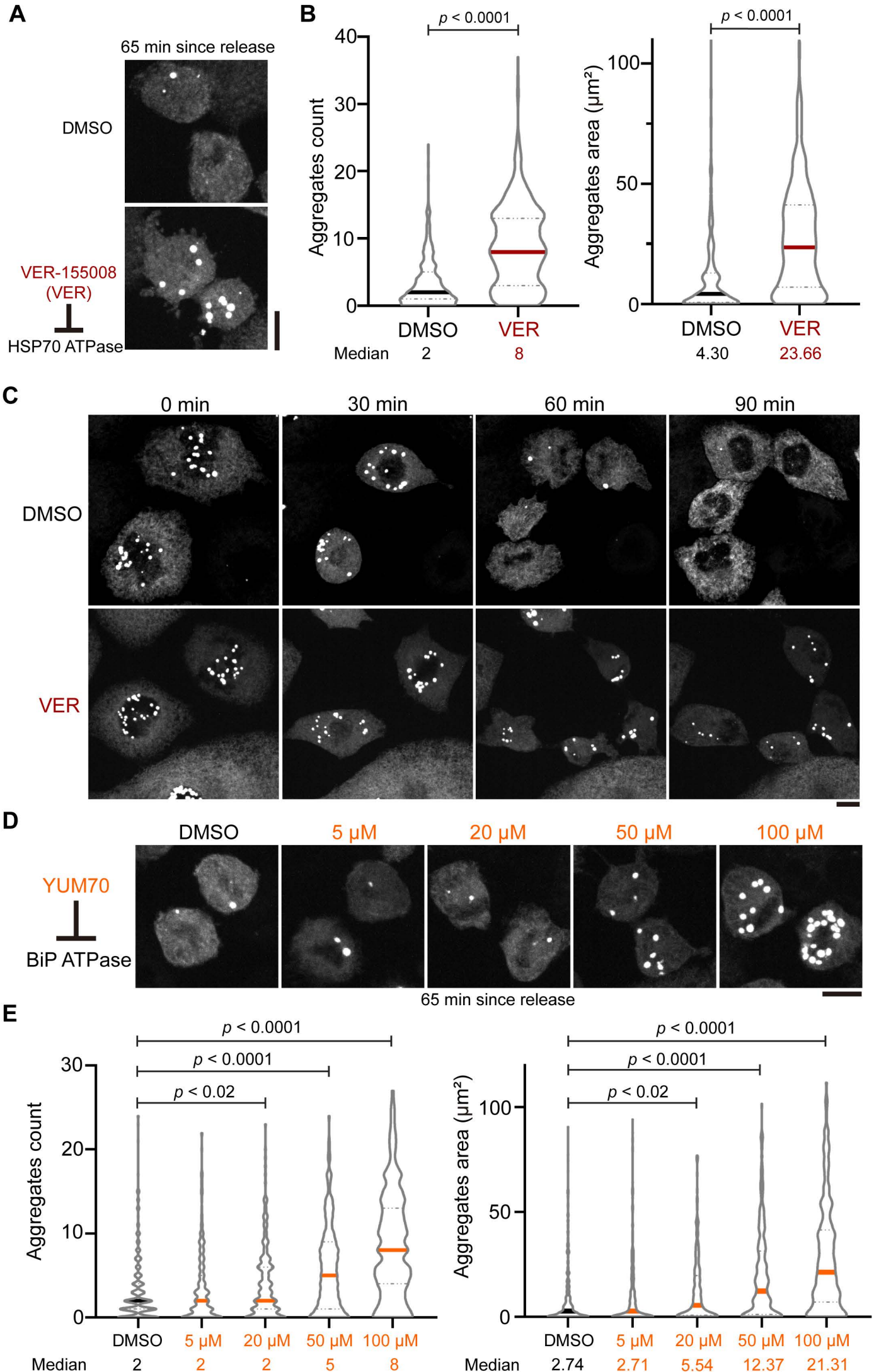
A
65 min since release
DMSO
VER-155008
(VER)
HSP70 ATPase
B
p < 0.0001
Aggregates count
DMSO
VER
Median
2
8
p < 0.0001
Aggregates area (µm²)
DMSO
VER
4.30
23.66
C
0 min
30 min
60 min
90 min
DMSO
VER
D
DMSO
5 µM
20 µM
50 µM
100 µM
YUM70
BiP ATPase
65 min since release
E
p < 0.0001
p < 0.0001
p < 0.02
Aggregates count
DMSO
5 µM
20 µM
50 µM
100 µM
Median
2
2
2
5
8
p < 0.0001
p < 0.0001
p < 0.02
Aggregates area (µm²)
DMSO
5 µM
20 µM
50 µM
100 µM
Median
2.74
2.71
5.54
12.37
21.31

# Figure 6

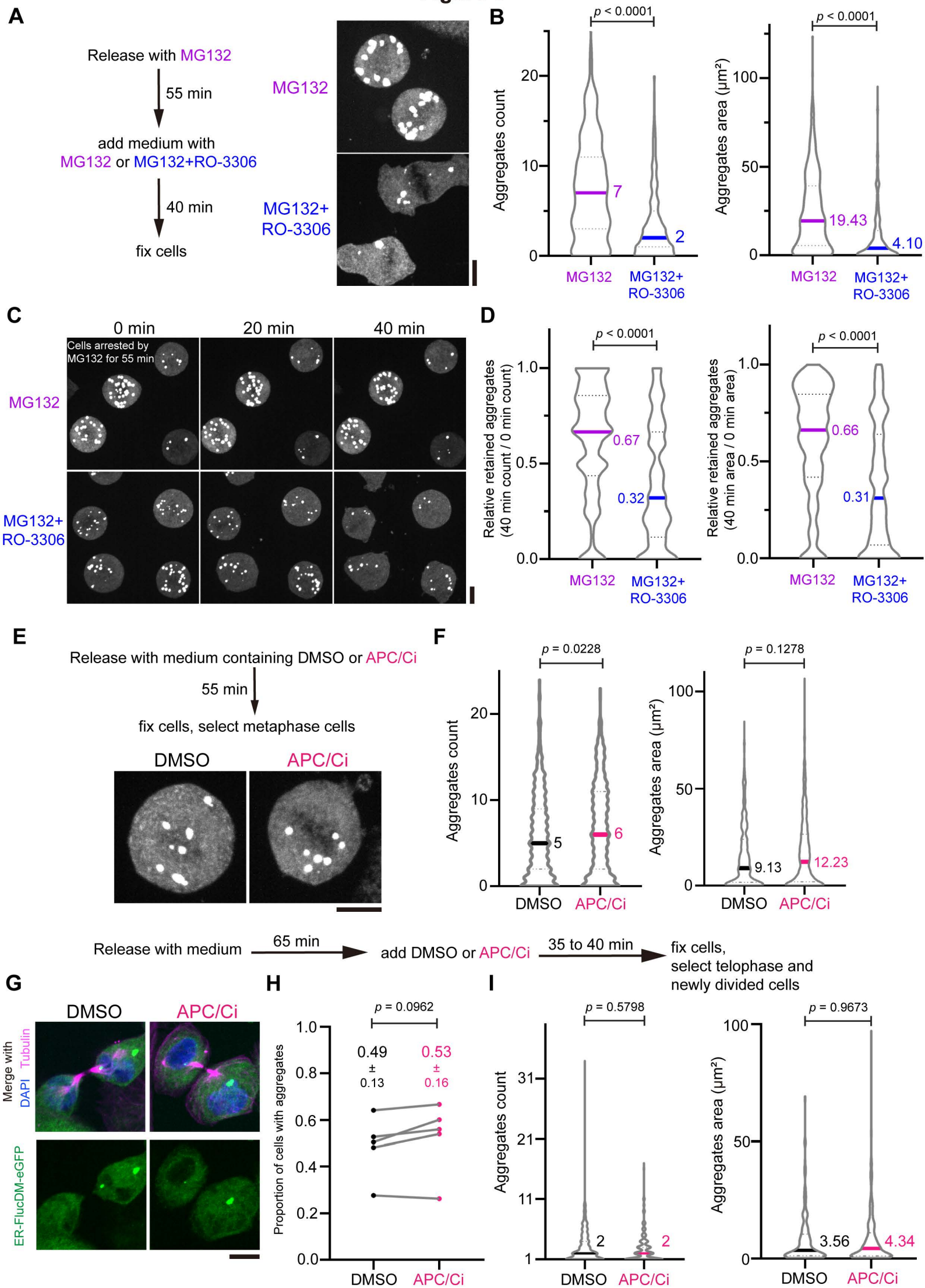
A
Release with MG132
55 min
add medium with
MG132 or MG132+RO-3306
40 min
fix cells
MG132
MG132+
RO-3306
B
p < 0.0001
Aggregates count
7
2
MG132
MG132+
RO-3306
p < 0.0001
Aggregates area (μm²)
19.43
4.10
MG132
MG132+
RO-3306
C
0 min
20 min
40 min
Cells arrested by
MG132 for 55 min
MG132
MG132+
RO-3306
D
p < 0.0001
Relative retained aggregates
(40 min count / 0 min count)
0.67
0.32
MG132
MG132+
RO-3306
p < 0.0001
Relative retained aggregates
(40 min area / 0 min area)
0.66
0.31
MG132
MG132+
RO-3306
E
Release with medium containing DMSO or APC/Ci
55 min
fix cells, select metaphase cells
DMSO
APC/Ci
F
p = 0.0228
Aggregates count
5
6
DMSO
APC/Ci
p = 0.1278
Aggregates area (μm²)
9.13
12.23
DMSO
APC/Ci
Release with medium
65 min
add DMSO or APC/Ci
35 to 40 min
fix cells,
select telophase and
newly divided cells
G
DMSO
APC/Ci
Merge with
DAPI Tubulin
ER-FlucDM-eGFP
H
p = 0.0962
Proportion of cells with aggregates
0.49
±
0.13
0.53
±
0.16
DMSO
APC/Ci
I
p = 0.5798
Aggregates count
2
2
DMSO
APC/Ci
p = 0.9673
Aggregates area (μm²)
3.56
4.34
DMSO
APC/Ci

# Figure 7

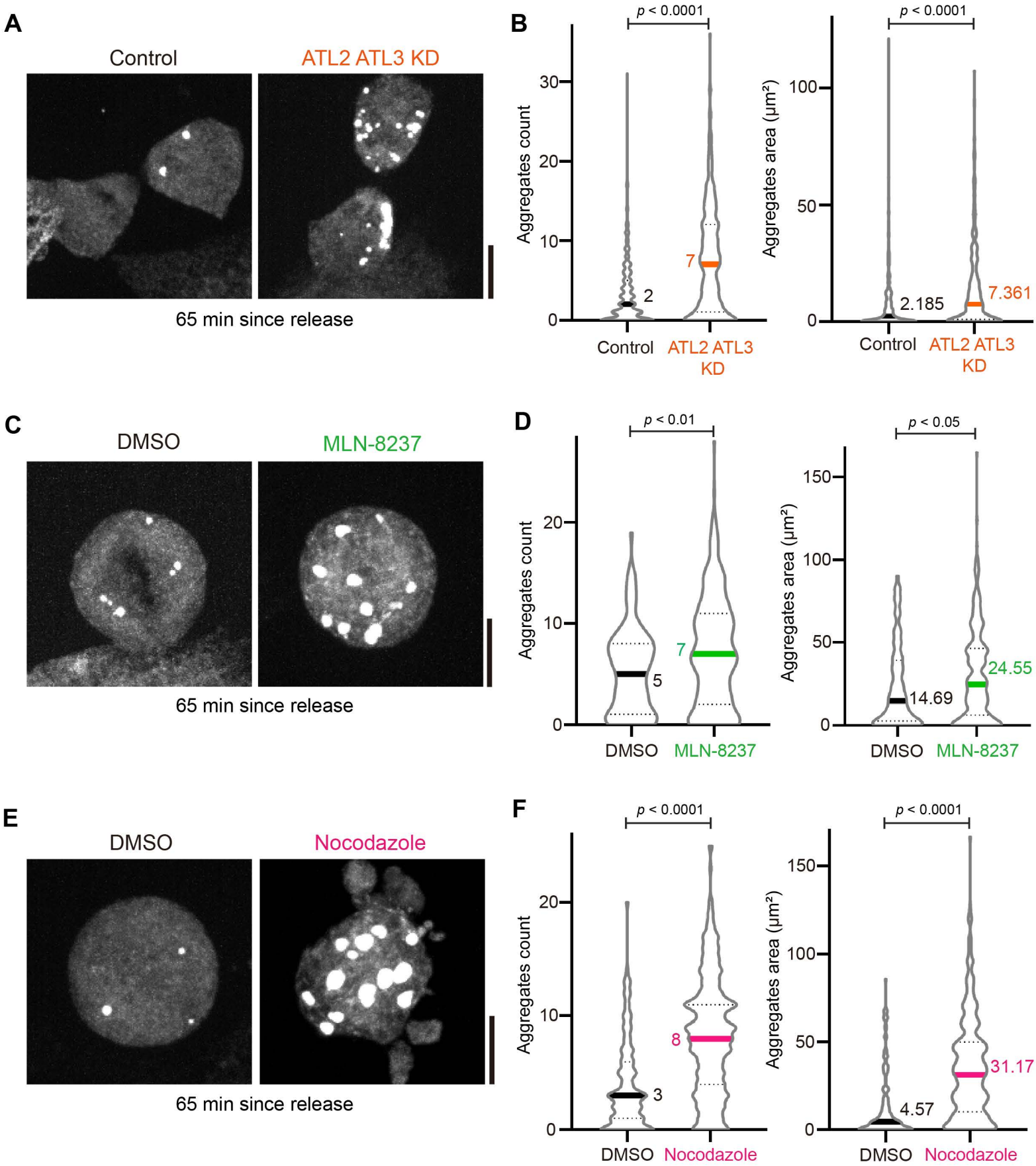
A
Control
ATL2 ATL3 KD
65 min since release
B
p < 0.0001
Aggregates count
30
20
10
0
7
2
Control
ATL2 ATL3 KD
p < 0.0001
Aggregates area (µm²)
100
50
0
2.185
7.361
Control
ATL2 ATL3 KD
C
DMSO
MLN-8237
65 min since release
D
p < 0.01
Aggregates count
20
10
0
7
5
DMSO
MLN-8237
p < 0.05
Aggregates area (µm²)
150
100
50
0
24.55
14.69
DMSO
MLN-8237
E
DMSO
Nocodazole
65 min since release
F
p < 0.0001
Aggregates count
20
10
0
8
3
DMSO
Nocodazole
p < 0.0001
Aggregates area (µm²)
150
100
50
0
31.17
4.57
DMSO
Nocodazole

# Figure S1

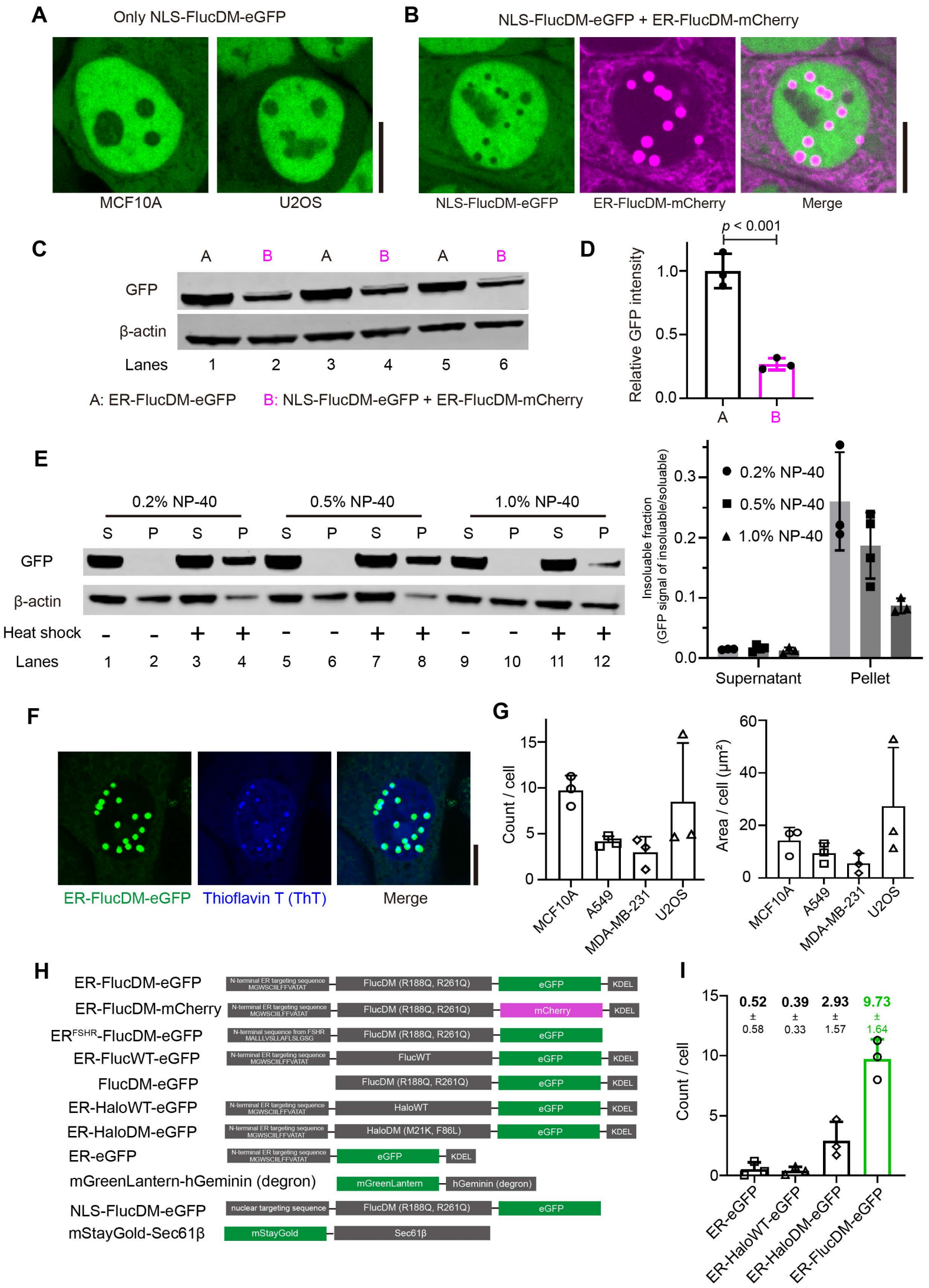
A
Only NLS-FlucDM-eGFP
MCF10A
U2OS
B
NLS-FlucDM-eGFP + ER-FlucDM-mCherry
NLS-FlucDM-eGFP
ER-FlucDM-mCherry
Merge
C
A B A B A B
GFP
β-actin
Lanes 1 2 3 4 5 6
A: ER-FlucDM-eGFP
B: NLS-FlucDM-eGFP + ER-FlucDM-mCherry
D
p < 0.001
Relative GFP intensity
1.0
0.5
0.0
A
B
E
0.2% NP-40
0.5% NP-40
1.0% NP-40
S P S P S P S P S P S P
GFP
β-actin
Heat shock - - + + - - + + - - + +
Lanes 1 2 3 4 5 6 7 8 9 10 11 12
Insoluable fraction
(GFP signal of insoluable/soluable)
0.3
0.2
0.1
0.0
0.2% NP-40
0.5% NP-40
1.0% NP-40
Supernatant
Pellet
F
ER-FlucDM-eGFP
Thioflavin T (ThT)
Merge
G
Count / cell
15
10
5
0
MCF10A
A549
MDA-MB-231
U2OS
Area / cell (μm²)
60
40
20
0
MCF10A
A549
MDA-MB-231
U2OS
H
ER-FlucDM-eGFP
N-terminal ER targeting sequence MGWSCIILFFVATAT
FlucDM (R188Q, R261Q)
eGFP
KDEL
ER-FlucDM-mCherry
N-terminal ER targeting sequence MGWSCIILFFVATAT
FlucDM (R188Q, R261Q)
mCherry
KDEL
ERFSHR-FlucDM-eGFP
N-terminal sequence from FSHR MALLLVSLLAFLSLGSG
FlucDM (R188Q, R261Q)
eGFP
ER-FlucWT-eGFP
N-terminal ER targeting sequence MGWSCIILFFVATAT
FlucWT
eGFP
KDEL
FlucDM-eGFP
FlucDM (R188Q, R261Q)
eGFP
KDEL
ER-HaloWT-eGFP
N-terminal ER targeting sequence MGWSCIILFFVATAT
HaloWT
eGFP
KDEL
ER-HaloDM-eGFP
N-terminal ER targeting sequence MGWSCIILFFVATAT
HaloDM (M21K, F86L)
eGFP
KDEL
ER-eGFP
N-terminal ER targeting sequence MGWSCIILFFVATAT
eGFP
KDEL
mGreenLantern-hGeminin (degron)
mGreenLantern
hGeminin (degron)
NLS-FlucDM-eGFP
nuclear targeting sequence
FlucDM (R188Q, R261Q)
eGFP
mStayGold-Sec61β
mStayGold
Sec61β
I
Count / cell
15
10
5
0
0.52 ± 0.58
0.39 ± 0.33
2.93 ± 1.57
9.73 ± 1.64
ER-eGFP
ER-HaloWT-eGFP
ER-HaloDM-eGFP
ER-FlucDM-eGFP

# Figure S2

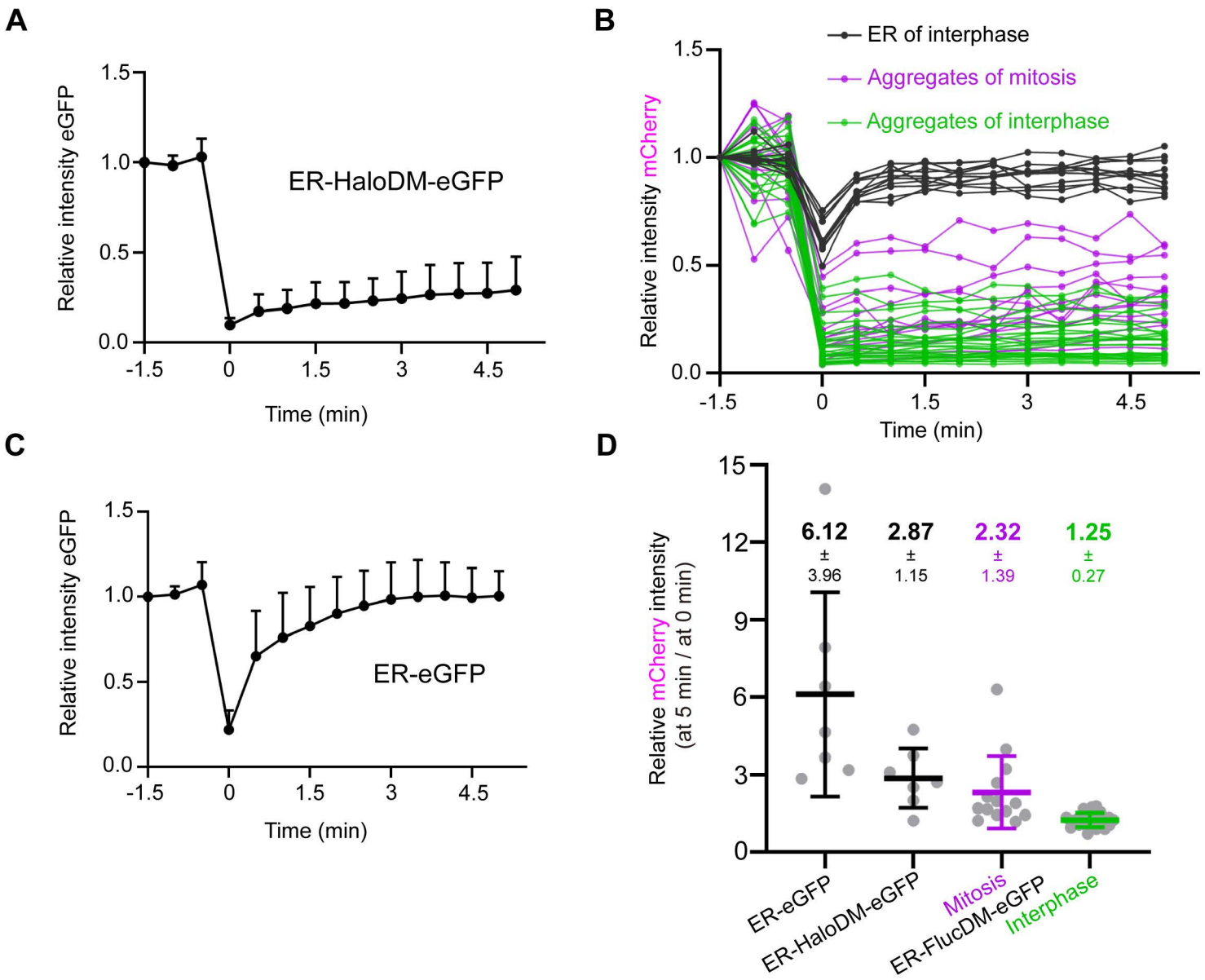
A
Relative intensity eGFP
ER-HaloDM-eGFP
Time (min)
B
ER of interphase
Aggregates of mitosis
Aggregates of interphase
Relative intensity mCherry
Time (min)
C
Relative intensity eGFP
ER-eGFP
Time (min)
D
Relative mCherry intensity
(at 5 min / at 0 min)
6.12 ± 3.96
2.87 ± 1.15
2.32 ± 1.39
1.25 ± 0.27
ER-eGFP
ER-HaloDM-eGFP
Mitosis
ER-FlucDM-eGFP
Interphase

# Figure S3

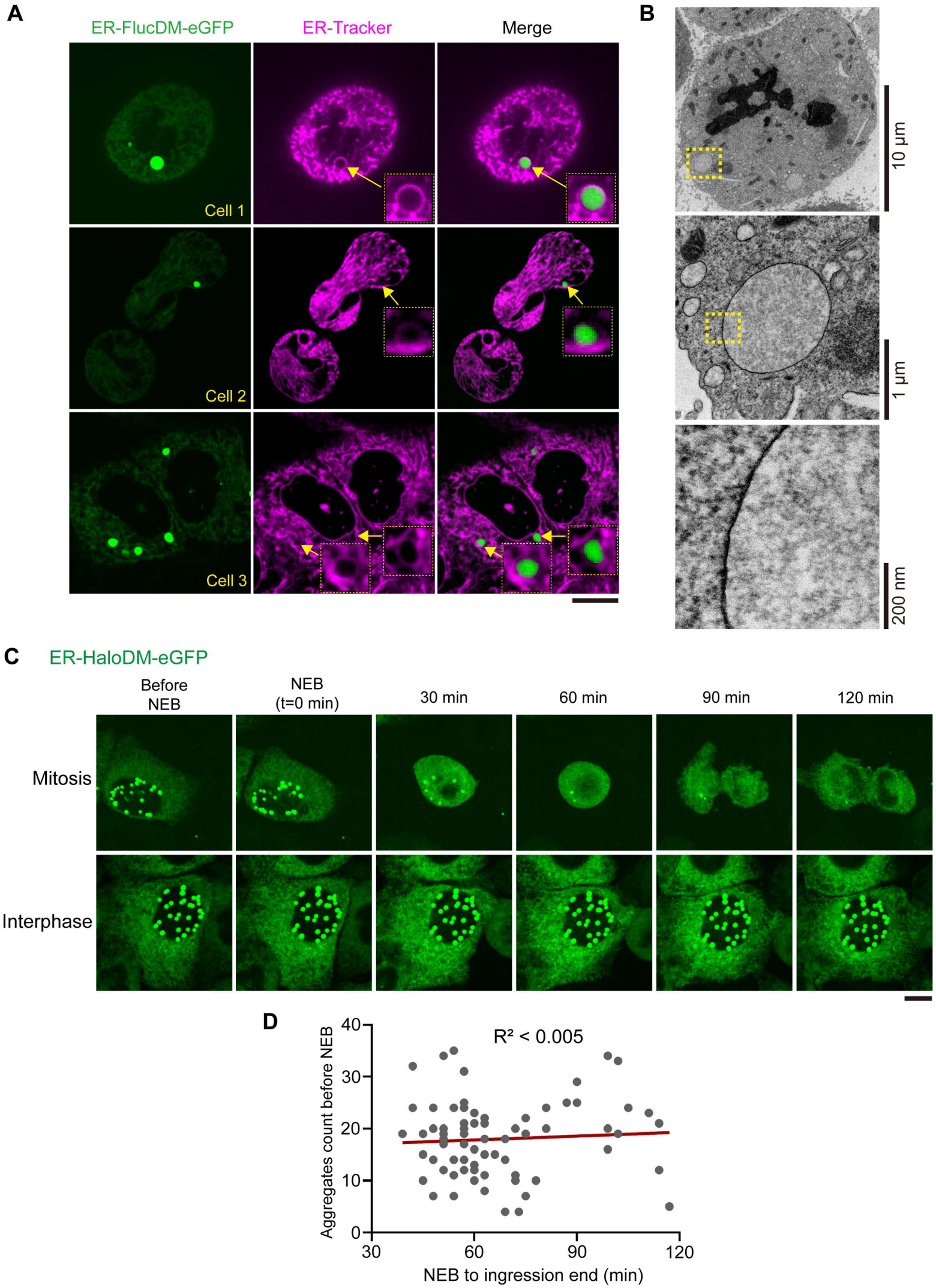
A
ER-FlucDM-eGFP
ER-Tracker
Merge
Cell 1
Cell 2
Cell 3
B
10 µm
1 µm
200 nm
C
ER-HaloDM-eGFP
Before NEB
NEB (t=0 min)
30 min
60 min
90 min
120 min
Mitosis
Interphase
D
R² < 0.005
Aggregates count before NEB
NEB to ingression end (min)
0
10
20
30
40
30
60
90
120

# Figure S4

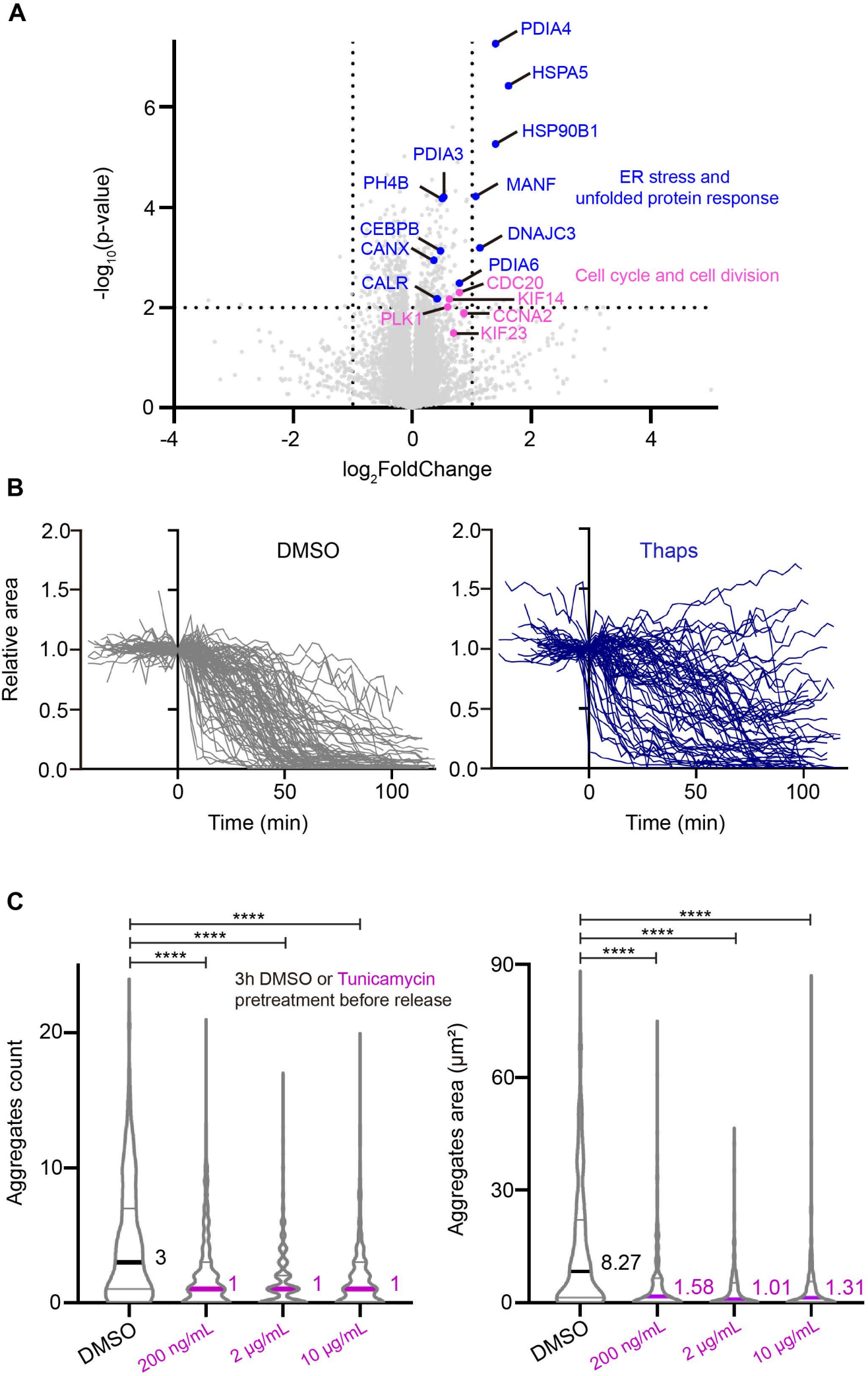
A
PDIA4
HSPA5
HSP90B1
PDIA3
PH4B
MANF
ER stress and
unfolded protein response
CEBPB
CANX
DNAJC3
PDIA6
CALR
CDC20
Cell cycle and cell division
KIF14
PLK1
CCNA2
KIF23
-log10(p-value)
log2FoldChange
B
DMSO
Thaps
Relative area
Time (min)
C
3h DMSO or Tunicamycin
pretreatment before release
Aggregates count
Aggregates area (µm²)
****
3
1
8.27
1.58
1.01
1.31
DMSO
200 ng/mL
2 µg/mL
10 µg/mL

# Figure S5

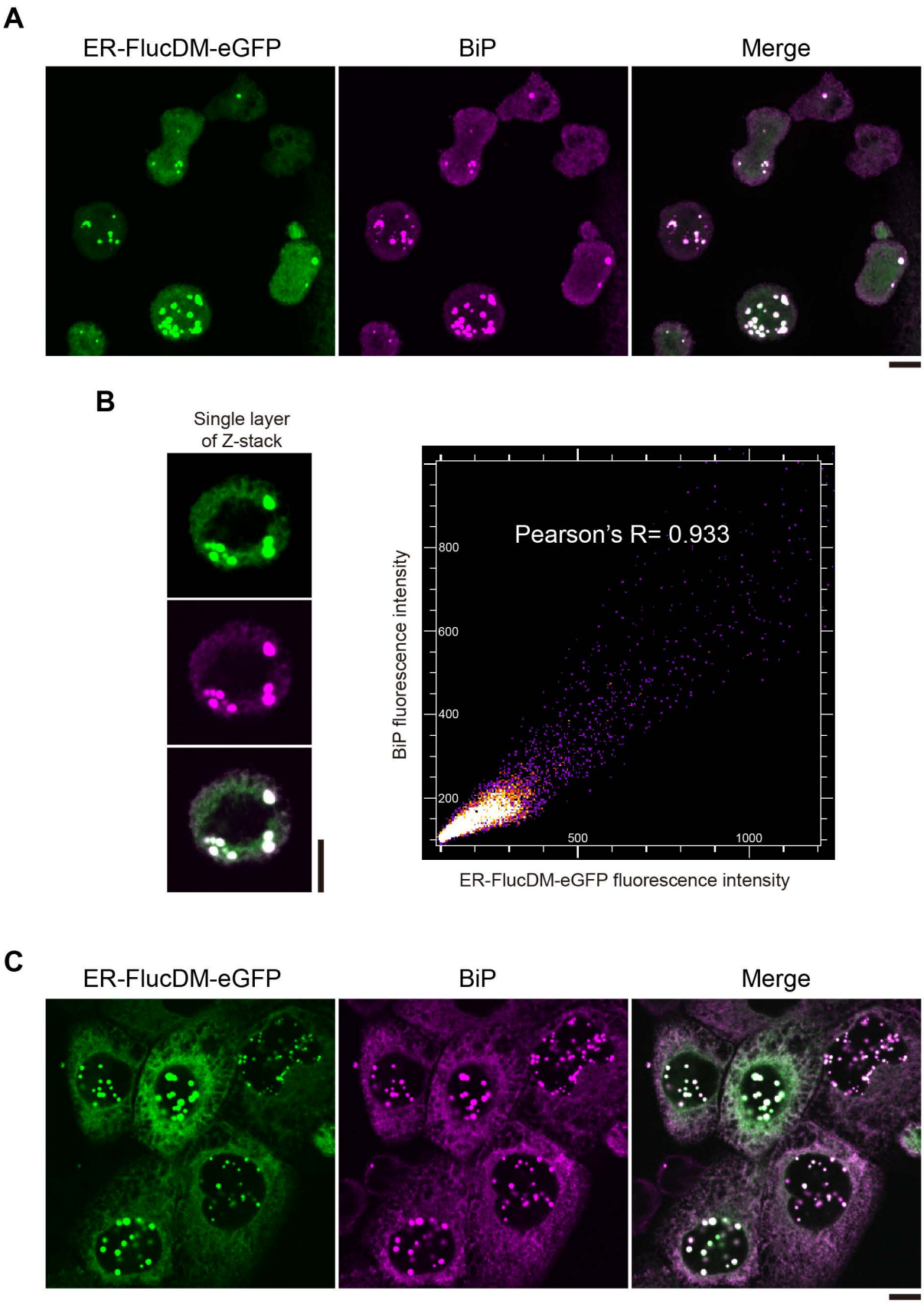
A
ER-FlucDM-eGFP
BiP
Merge
B
Single layer
of Z-stack
Pearson's R= 0.933
BiP fluorescence intensity
800
600
400
200
500
1000
ER-FlucDM-eGFP fluorescence intensity
C
ER-FlucDM-eGFP
BiP
Merge

# Figure S6

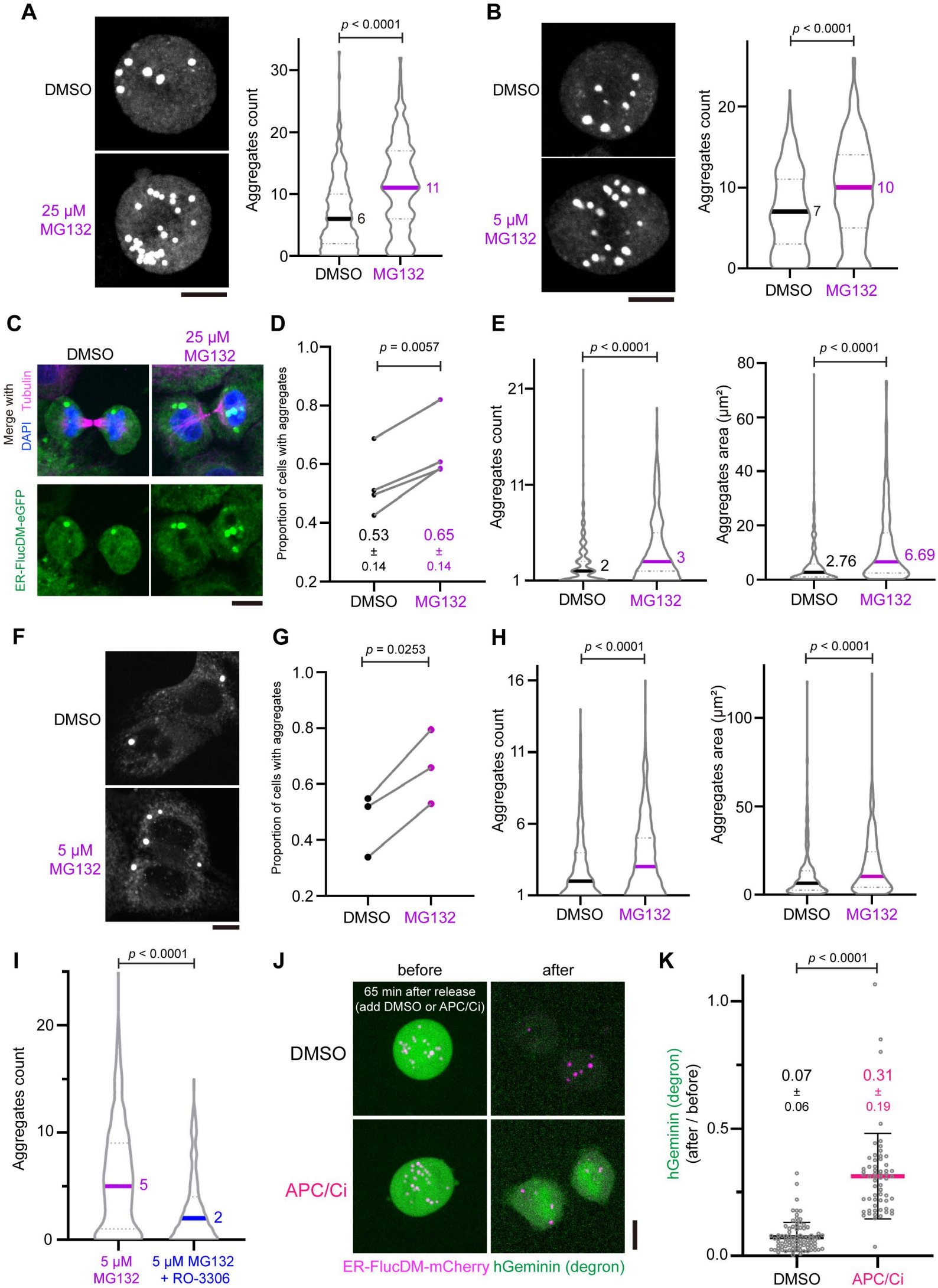
A
DMSO
25 μM MG132
p < 0.0001
Aggregates count
6
11
DMSO
MG132
B
DMSO
5 μM MG132
p < 0.0001
Aggregates count
7
10
DMSO
MG132
C
DMSO
25 μM MG132
Merge with DAPI Tubulin
ER-FlucDM-eGFP
D
p = 0.0057
Proportion of cells with aggregates
0.53 ± 0.14
0.65 ± 0.14
DMSO
MG132
E
p < 0.0001
Aggregates count
2
3
p < 0.0001
Aggregates area (μm²)
2.76
6.69
DMSO
MG132
F
DMSO
5 μM MG132
G
p = 0.0253
Proportion of cells with aggregates
DMSO
MG132
H
p < 0.0001
Aggregates count
p < 0.0001
Aggregates area (μm²)
DMSO
MG132
I
p < 0.0001
Aggregates count
5
2
5 μM MG132
5 μM MG132 + RO-3306
J
before
after
65 min after release (add DMSO or APC/Ci)
DMSO
APC/Ci
ER-FlucDM-mCherry
hGeminin (degron)
K
p < 0.0001
hGeminin (degron) (after / before)
0.07 ± 0.06
0.31 ± 0.19
DMSO
APC/Ci

# Figure S7

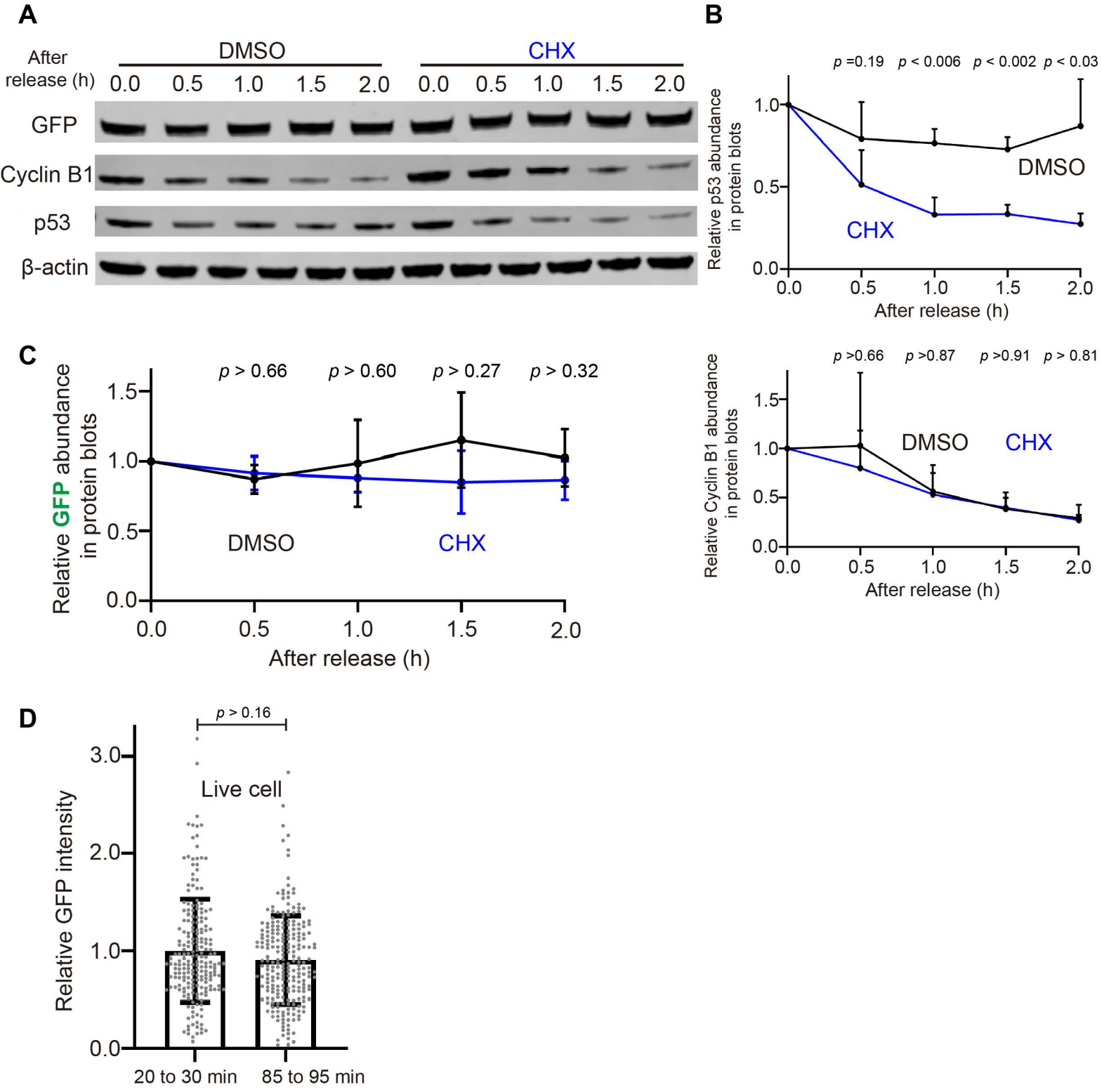
A
After release (h)
DMSO
CHX
0.0 0.5 1.0 1.5 2.0 0.0 0.5 1.0 1.5 2.0
GFP
Cyclin B1
p53
β-actin
B
p =0.19 p < 0.006 p < 0.002 p < 0.03
Relative p53 abundance in protein blots
DMSO
CHX
After release (h)
p >0.66 p >0.87 p >0.91 p > 0.81
Relative Cyclin B1 abundance in protein blots
DMSO
CHX
After release (h)
C
p > 0.66 p > 0.60 p > 0.27 p > 0.32
Relative GFP abundance in protein blots
DMSO
CHX
After release (h)
D
p > 0.16
Live cell
Relative GFP intensity
20 to 30 min
85 to 95 min